A Lorentz-Force Actuated Needle-Free Intraocular Injection Device

by

James White

Submitted to the Department of Mechanical Engineering
in partial fulfillment of the requirements for the degree of

Master of Science in Mechanical Engineering

at the

MASSACHUSETTS INSTITUTE OF TECHNOLOGY

June 2012

Author .....
Department of Mechanical Engineering
May 21, 2012

Certified by .....
Ian W. Hunter
Hatsopoulos Professor of Mechanical Engineering
Thesis Supervisor

Accepted by .....
David E. Hardt
Chairman, Department Committee on Graduate Students

A Lorentz-Force Actuated Needle-Free Intraocular Injection Device

by

James White

Submitted to the Department of Mechanical Engineering
on May 23, 2012, in partial fulfillment of the
requirements for the degree of
Master of Science in Mechanical Engineering

Abstract

Intravitreal injection is a common treatment in ophthalmology, but it can lead to considerable patient anxiety and numerous complications. Lorentz-force actuated needle-free jet injection has been shown to successfully deliver fluid to various layers of skin, and, by its nature, may reduce intravitreal injection anxiety and complications. The challenges of adapting current Lorentz-force actuated needle-free jet injection technology to intravitreal injection were investigated using a previously developed jet injection system. Two iterations of an intravitreal injection-specific control scheme were designed, implemented, and tested. Several tools were developed in tandem with the research, including intravitreal injection 3D reconstruction software, actuator-jet transfer function generation software, and bench-top eye injection staging equipment. From injection trials into *ex vivo* rabbit eyes, we find that needle-free jet injection can be used for intravitreal drug delivery. The new system is capable of delivering 40 µL of fluid to the posterior vitreous humor, with an injection duration less than 100 ms and scleral entry site less than 350 µm in diameter. A relationship has been developed between injection parameters and eye damage metrics that can be used for future parameter optimization, minimizing damage to the eye.

Thesis Supervisor: Ian W. Hunter
Title: Hatsopoulos Professor of Mechanical Engineering

Acknowledgments

Thank you to my parents, for being patient when I needed time, tough when I needed advice (even if I didn't know it), and loving every second for the last 23 years. You pulled me through circumstances where the odds were against me, and I wouldn't be as fulfilled or inspired as I am today without you. Our relationship has changed and grown for the better as far back as I can remember, and I can't wait to see the amazing life you continue to make for yourselves, while sharing with you my own adventures.

Thank you to all of my teachers, grade school through graduate school, that have bestowed their own intense academic and artistic curiosity to me. Most especially, thank you to Prof. Ian Hunter, who has equipped me not only with knowledge and skills through his diverse and collaborative laboratory environment but also with the excitement for discovery and creation that he constantly emanates. I will keep the philosophy of the BioInstrumentation Lab in my thoughts wherever my future endeavors lead me.

Thank you to all of my colleagues, who have often played the roles of mentors and friends, including Cathy Hogan, Jean Chang, Adam Wahab, Ellen Chen, Bryan Ruddy, and the rest of the BioInstrumentation Lab. I'll remember you forever for your exceptional abilities, sincere advice, and stimulating conversation. However, I'm still waiting on that Hendrick's Gin you promised me (you know who you are).

Finally, thank you to the friends, foes, beautiful women, striking men, roommates, strangers, and combinations thereof that have shaped me over the years. Special thanks goes to my current apartment-mates and partners-in-crime, Praveen Subramani, Richard Whalley, and Dmitry Ter-Ovanesyan. From washing the dishes I forgot about to being a part of our fledgling start-up, you have kept me sane and have helped me realize which parts of life have real importance.

Contents

List of Figures

Chapter 1

Introduction

Intravitreal injection is a necessary procedure for treatment of eye diseases such as age-related macular degeneration [10], proliferative diabetic retinopathy [11], and endophthalmitis [12]. The procedure demands constant focus and dexterity from an ophthalmologist. Mistakes are uncommon but can lead to serious complications [13] such as lens damage, retinal damage, infection, and even ocular explosion [14]. Repeated injections are often required for months or a patient's entire life, and patient compliance with this regimen leads to better visual health. However, discomfort and anxiety associated with the operation is common to all injections [15].

A cost-effective injection system that reduces the frequency of complications and increases patient compliance would transform eye care, and the development of such a system was the goal of this thesis project. This thesis explains current intravitreal injection techniques, eye biomechanics, prior jet injection development, and eye experimentation methodology. Next, preliminary experiments with current jet injection technology are analyzed. Finally, we present the design, development, and testing of a new intravitreal jet injector and the future work needed to bring the device to its full potential.

Chapter 2

Background

2.1 Intravitreal Injection

2.1.1 Introduction

The vitreous body or humor occupies the majority of the volume of the human eye, shown in Fig. 2-1. Several methods have been used for prolonged drug delivery to the vitreous humor, such as topical application, implantable devices, microspheres, and liposomes. However, regularly administered intravitreal needle injections remain the most common because they are the most direct and immediate route of drug delivery. The goal of an intravitreal injection is to deposit drug inside the vitreous humor, while causing minimal damage to surrounding tissues, including the lens, retina, cornea, choroid, and sclera.

2.1.2 Biomechanics

The structure of the eye in the injection area makes this type of injection more difficult and risky than a typical intramuscular or intravenous injection. In a correctly performed intravitreal injection, the needle pierces the sclera, choroid, and vitreous humor, while remaining posterior to the limbus and ciliary bodies and anterior to the *ora serrata*. This path is shown in Fig. 2-2. The *ora serrata* is the area where the retina ends. In Fig. 2-3, the structure of the injection site is on the anterior side of

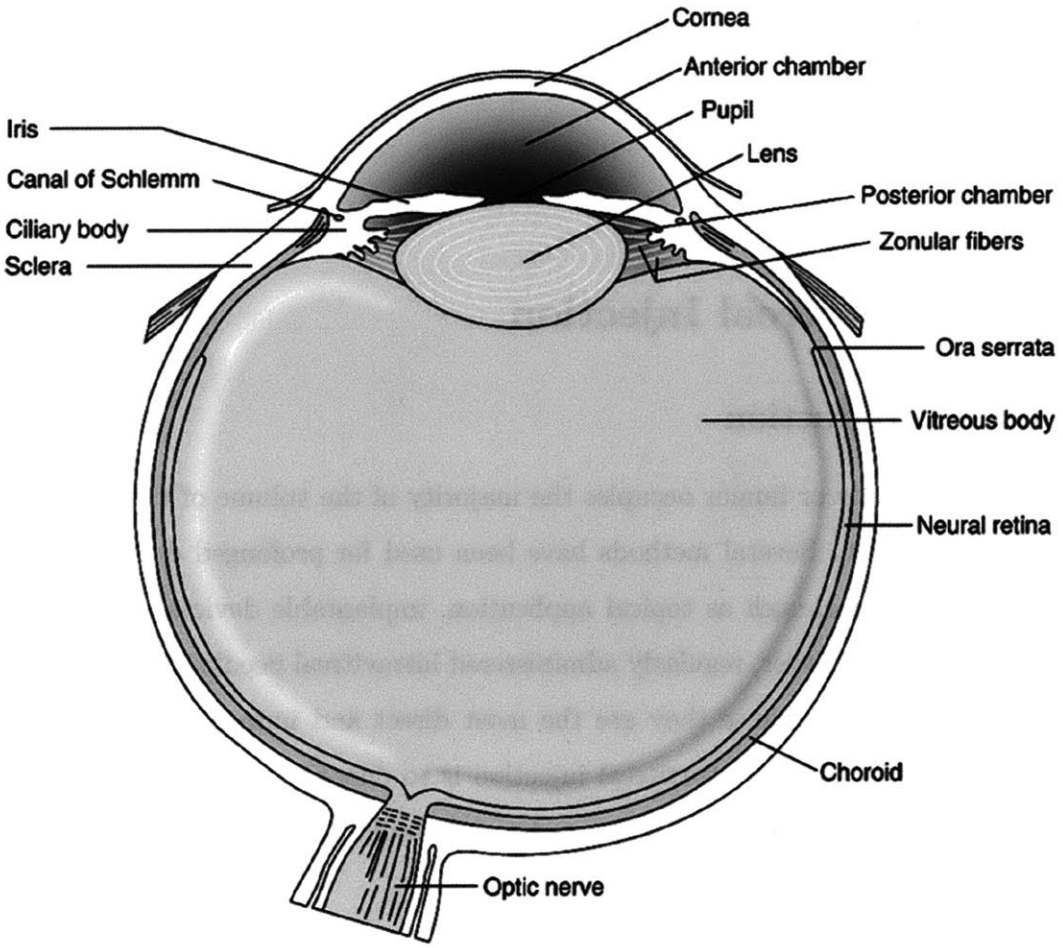

Figure 2-1: Diagram of the human eye from communications with Institut de la Vision [1] & Sanofi Fovea; superior view of right eye.

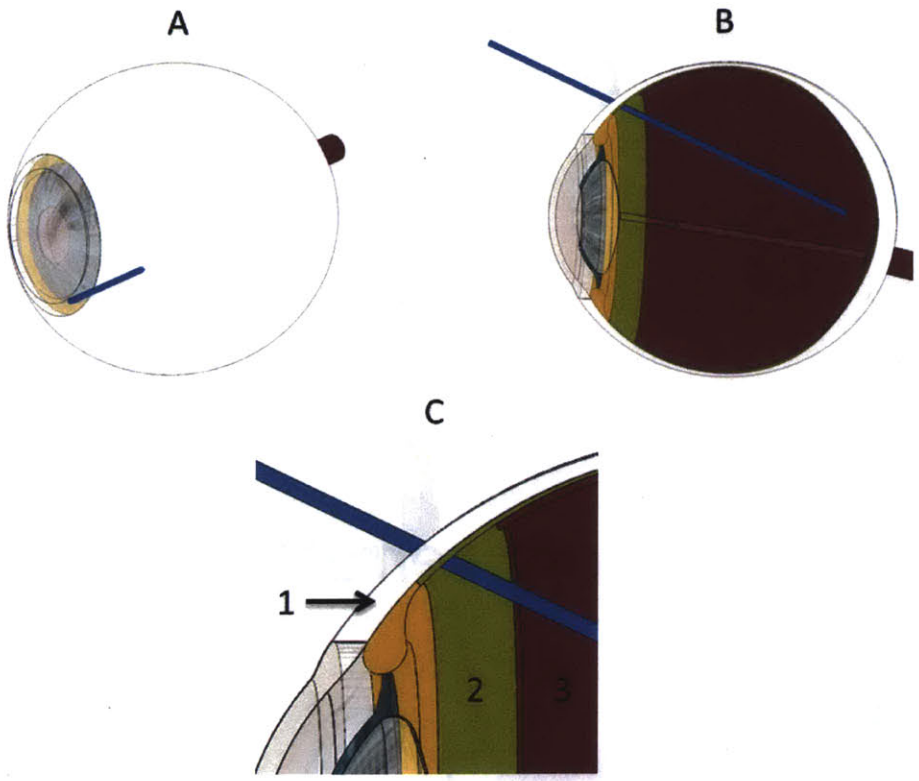

Figure 2-2: SolidWorks model of the human eye with the path of intravitreal injection shown. (a) Complete eye from superior lateral view. (b) Cross-section of eye along injection path. (c) Simplified injection site structure: (1) sclera, (2) choroid, (3) retina.

the *ora serrata*, while the retina is on the posterior side.

The biomechanical properties of these structures have been studied previously. For example, the force required by a 260.4 µm diameter needle (31-gauge) to penetrate an enucleated sclera was found to be about 0.3 N [16]. Larger (lower gauge) needles require more force, result in more reflux after the injection, and are associated with more pain [17]. The sclera is about 0.5 mm thick [18], with a modulus of elasticity of $2.3 \times 10^6\,\mathrm{N/m^2}$ [19]. In the injection area, the choroid is about five times less stiff than the sclera and about three times less thick [20]. The sclera is thus the most resistant layer for any injection to pierce.

The vitreous humor is a clear gel-liquid hybrid that fills the eye cavity posterior to the lens. Its structure is a double-network, consisting of randomly spaced collagen

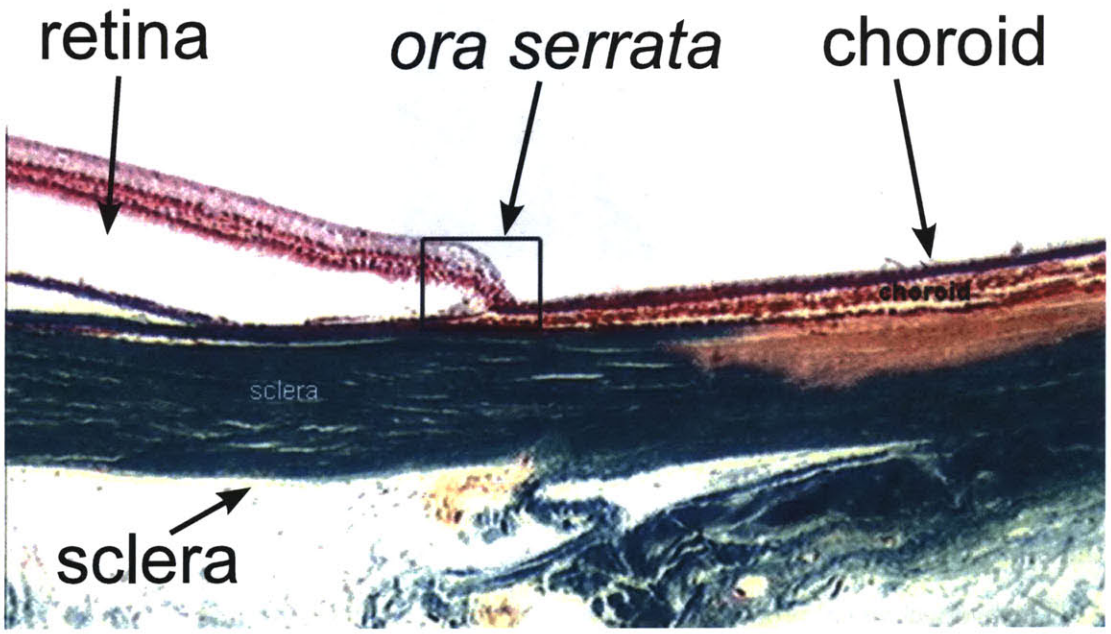

Figure 2-3: Histology of the *ora serrata*, with the posterior eye to the left and the anterior eye to the right. Edited image from the instructional materials of the Department of Neurobiology, School of Medicine, University of California, Los Angeles[2]. To prevent damage to the retina, injection must occur anterior to the *ora serrata*.

fibers and macromolecules of hyaluronic acid [21]. It is believed that the hyaluronic network is responsible for the vitreous resistance to sudden shock and that the collagen network is responsible for the vitreous tensile strength.

Transport in the vitreous is estimated to be 30% convection and 70% diffusion for small molecules like acid orange 8, with a molecular weight of 364.4 D and a half-life in the vitreous on the order of hours [22]. However, modern (and most commonly used) drugs such as bevacizumab (Avastin), with molecular weights above 1000 kD, can have half-lives of four days. For high molecular weight drugs, convection is estimated to be much more influential than diffusion [23]. Convection currents are caused by several mechanisms in the eye, including aqueous outflow in the anterior sections of the eye and vitreous outflow in the posterior. The result of a vitreous flow simulation that agrees with experimental data on the rabbit eye is shown in Fig. 2-4. Because high molecular weight drugs diffuse very slowly, positioning them in high concentrations near a target site is ideal. Traditional intravitreal needle injections do not have this capability.

2.1.3 Technique

Guidelines for intravitreal injection have been published, but technique still varies considerably between ophthalmologists [24]. Normally, a 260.4 µm–412.8 µm diameter needle (27- to 31-gauge) is inserted about 3 mm posterior to the *limbus corneae* (the border of the cornea). Common injection volumes range from 50 µL to 150 µL. Before, after, and during the injection, meticulous care must be taken in order to minimize the risk of infection, of physically damaging the eye, and of causing the patient more pain than necessary [25]. A demonstration of the injection step of the procedure is shown in Fig. 2-5.

After an injection, a test for sensitivity to light and an intraocular pressure (IOP) measurement are taken. Abnormalities in these tests or symptoms reported by the patient are signs of complications with the injection. Complications are often only discovered at a subsequent appointment while imaging the fundus or testing visual acuity.

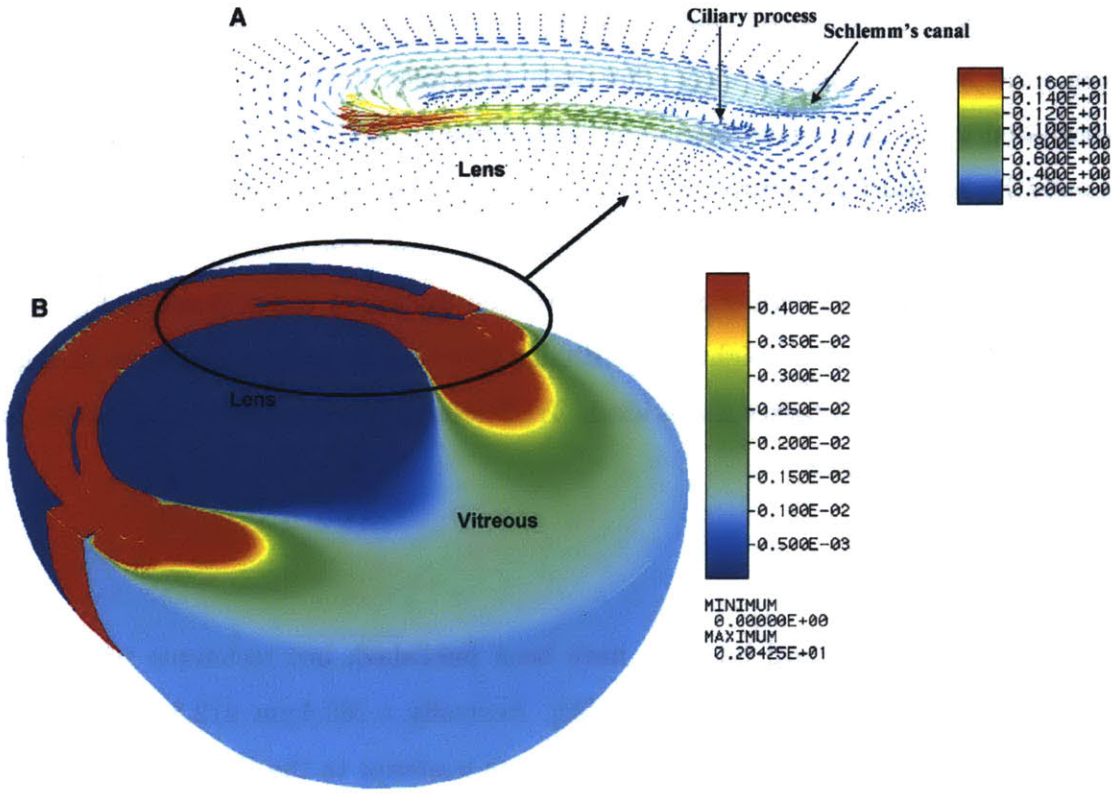

Figure 2-4: Speed contour and velocity vector for vitreous flow simulation in a rabbit eye, taken from J. Park et al. [3]. (Vitreous outflow of 0.1 µL/min) (A) Velocity vector plot for aqueous humor generated from ciliary processes and cleared through Schlemms canal. (B) Speed contour in anterior and posterior segments of the rabbit eye.

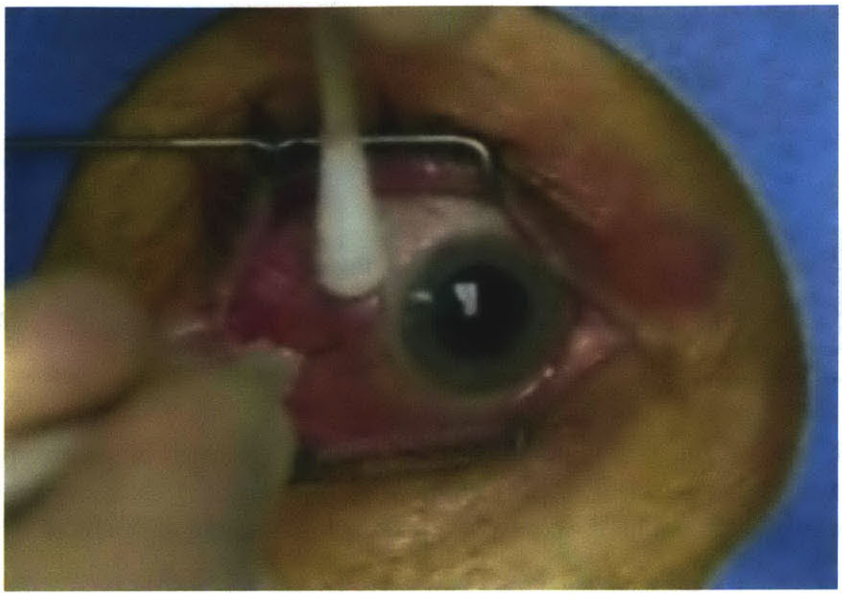

Figure 2-5: Frame from an intravitreal injection demonstration video created by James Folk[4].

2.2 Needle-Free Jet Injection Technology

Lorentz-force actuated needle-free jet injection (JI) technology developed at the MIT BioInstrumentation Lab [26] was identified as a promising solution to the complications and anxiety associated with needle intravitreal injection. The device works on the principle of the Lorentz force, a force exerted on a charged particle moving in a magnetic field. By running electrical current through a coil in a magnetic field, a force is generated. This force is transmitted through a piston to accelerate fluid up to velocities high enough to penetrate tissue.

A previous JI system is shown in Fig. 2-6. In the injector device, voltage is controlled across a voice coil which slides along a fixed magnet. A LabVIEW [27] program and data acquisition system actively monitor the position of the coil with a potentiometer and adjust the voltage to follow a pre-set path. The coil is attached to a syringe which ejects drug through a small nozzle at high speeds. The nozzle is placed in contact with tissue and the injection is initiated with a button.

Much of the design work in this thesis builds on the previously-developed JI device [5], the characteristics of which are discussed in the following sections.

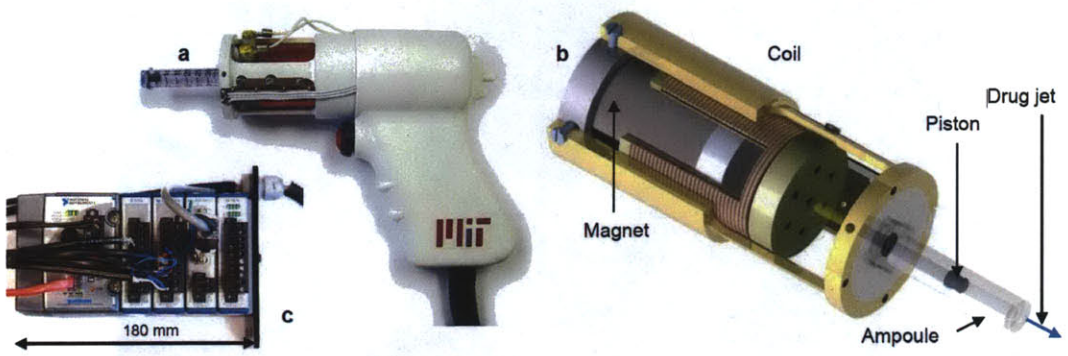

Figure 2-6: MIT Bioinstrumentation Lab's previous jet injector prototype. Picture taken from A. Taberner et al. [5].(a) Hand-held injector. (b) Cutaway view of linear Lorentz-force motor. (c) cRIO controller programmed using LabVIEW.

2.2.1 Electromechanical Design

The injector's chassis is steel and encloses the coil-magnet system. NdFeB magnets are fastened to a steel backplate. A moving voice coil is created by winding copper wire around a high performance polymer material which has been machined to slide along the inside of the chassis. The performance material is also machined to connect to a slide potentiometer and the syringe piston of the injector. The slide potentiometer is used for real-time coil displacement measurement. The system was designed to incorporate Injex^{TM} injection ampoules (INJEX Pharma Ltd., Miama, FL), which consist of a syringe and syringe piston. The syringe barrel is fastened to the front of the device, and as the voice coil moves, the syringe piston, attached to the front of the moving coil, ejects or draws in fluid. A system cutaway is shown in Fig. 2-7.

2.2.2 Control Design

A diagram of the control architecture is shown in Fig. 2-8. A trajectory is generated based on the velocities desired throughout the injection and the total desired drug volume. The controller uses two components to follow the injection trajectory, a proportional-integral (PI) feedback controller and a feed-forward command based on velocity. The coil position is PI-controlled using the voltage from the slide potentiometer as a feedback variable. Based on previous steady-state velocity-voltage

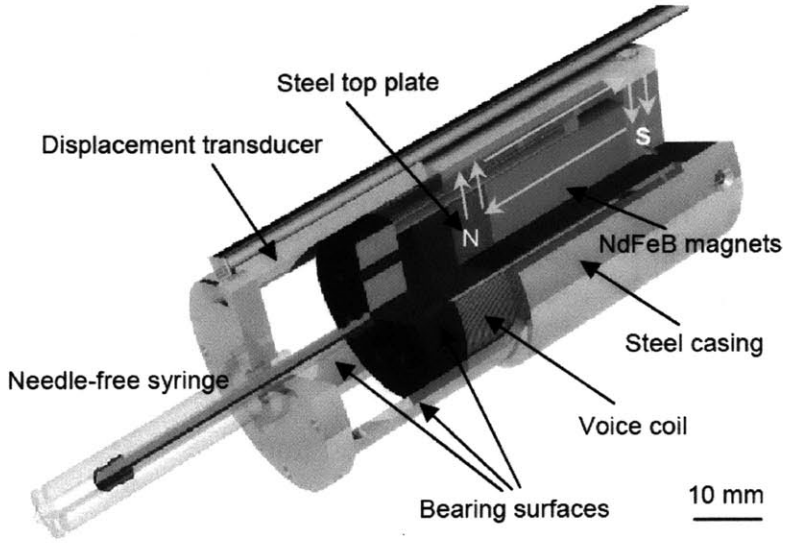

Figure 2-7: Cutaway view of the jet injector, taken from A. Taberner et al. [6].

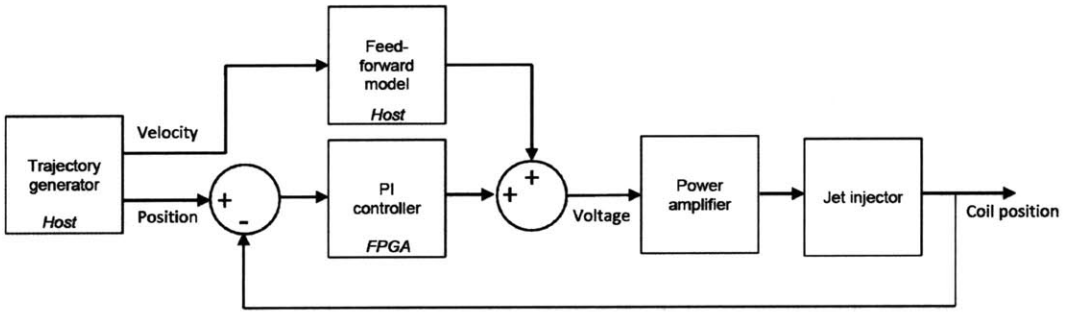

Figure 2-8: Jet injector control architecture, taken from A. Taberner et al. [6].

relationship calibrations and the velocity of the desired trajectory, a feed-forward voltage waveform is generated. Every time step, after controller calculations are completed in an FPGA, the total of the position feedback and feed-forward voltage are sent to the voltage input on a power amplifier. This amplifier drives the coil and ejects liquid from the ampoule.

2.2.3 Capabilities

Using Lorentz-force actuated JI technology, the jet velocity can be actively changed over the time of the injection by varying the current in the coil. Spring-loaded and

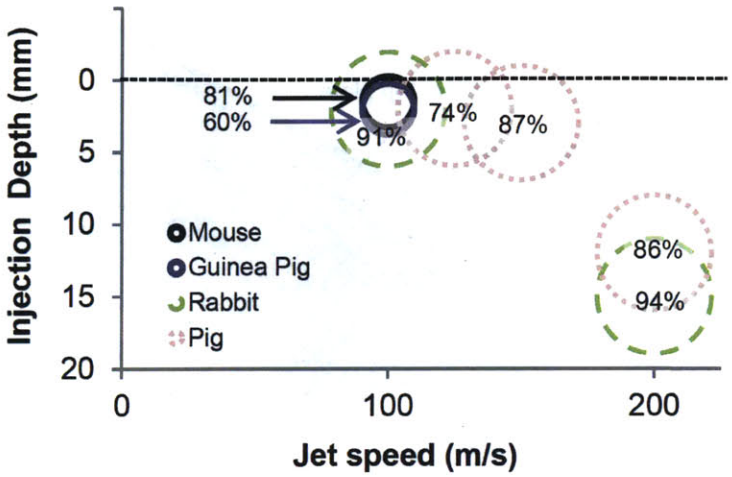

Figure 2-9: Injection depth for various jet injections into post-mortem tissues, taken from A. Taberner et al. [5]. The area of each circle represents the total desired injection volume (10 µL or 100 µL); the percentage quantifies the mean proportion of the drug absorbed by the tissue, by weight.

compressed-gas jet injectors do not have this ability. For example, the injection device can set a high velocity phase that pierces tissue followed by a low velocity phase to deliver the bulk of a drug. By varying the velocities in these two phases, a user can select the depth of the injection [28]. Depth of jet injection into tissues with varying injection settings are shown in Fig. 2-9. Moreover, dynamic delivery waveforms are possible using real-time position control. A representative waveform from the previous prototype is shown in Fig. 2-10. With position control, injections of set volumes are repeatable [5]. With previously tested devices, jets of fluid less than 100 µm in diameter are possible. An entire 100 µL injection can take place in less than 200 ms, followed by an automatic reload process. Injection velocities are able to reach over 200 m/s. Finally, the device is user-friendly, because one button can trigger the near-instantaneous injection waveform, requiring less dexterity than a traditional syringe.

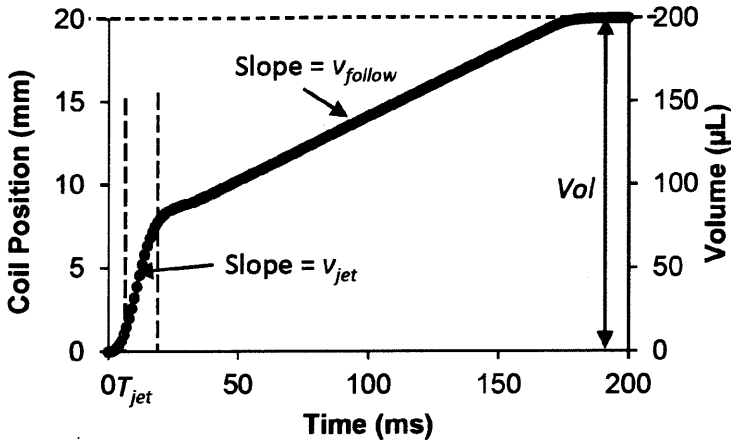

Figure 2-10: Sample position waveform of MIT Bioinstrumentation Lab's previous jet injector prototype, taken from A. Taberner et al. [5].

2.2.4 Applications to Intravitreal Injection

This technology was chosen for adaptation to intravitreal injections for a number of reasons. The absence of a needle anywhere inside the orbit prevents accidental stick wounds and decreases the risk of endophthalmitis. A velocity- and dosage-controlled delivery is only possible with an actuator and feedback control system and could ensure repeatable, accurate injections that target a specific depth in the eye. An assistant may be able to perform these injections with the addition of a user-friendly interface, saving valuable patient-ophthalmologist interaction time. Injections could also be performed more quickly and with less footprint than a needle, reducing patient anxiety and pain.

However, the structure of the eye in the injection path is much different than that of skin, the target of past JI testing. Successful delivery to the vitreous humor would require customization of the control strategy and possibly the nozzle geometry of the jet injector.

2.3 Intravitreal Jet Injection (IV JI) Previous Work

2.3.1 Accidental Injections

Because no jet injector has been approved for human intravitreal injection use, the only examples of human IV JI are accident reports. In two reported instances, the Dermojet jet injector has been used on the eyelid and accidentally pierced the sclera, continuing into the vitreous [7] [29]. The resultant injury from an accidental injection in 2009, shown in Fig. 2-11, caused diffuse vitreous hemorrhaging, which obscured the retina and acutely blinded the patient. In the examination following the event, the majority of the retina was found to be intact and the patient's IOP was normal. By the next day, the hemorrhage had cleared, revealing two retinal tears, which were treated. Ten months later, the tears had closed and the patient's vision was restored. In 1977 an accidental injection caused a retinal tear but had no lasting visual consequences. In both cases the injection entry and exit holes were at sites posterior to the ora serrata, which resulted in retinal tearing. If the injection site and speed could be controlled to eliminate entry and exit wounds being created, retinal tears and hemorrhaging may not have occurred at all.

2.3.2 Microneedle-Assisted Jet Injection

The only previous work found on IV JI development is the hybrid needle-jet system shown in Fig. 2-12 [8]. A microneedle (412.8 µm diameter, 27-gauge needle, protruding 0.1 mm from a flange) was fitted to the end of a Dermojet spring-powered jet injector. When inserted into the sclera at the normal intravitreal injection site, the needle penetrates less than 0.1 mm. The remaining piercing depth is eroded by the Dermojet jet. Test injections of 200 µL were run on both dissected and live rabbit eyes. No macroscopic or microscopic damage was reported. *In vivo* cross sections are shown in Fig. 2-13. Although this injector is a promising example of IV JI, it still suffers from many of the same disadvantages associated with needle injection, such as risk of scleral damage and infection, likely patient discomfort (especially using a 412.8 µm

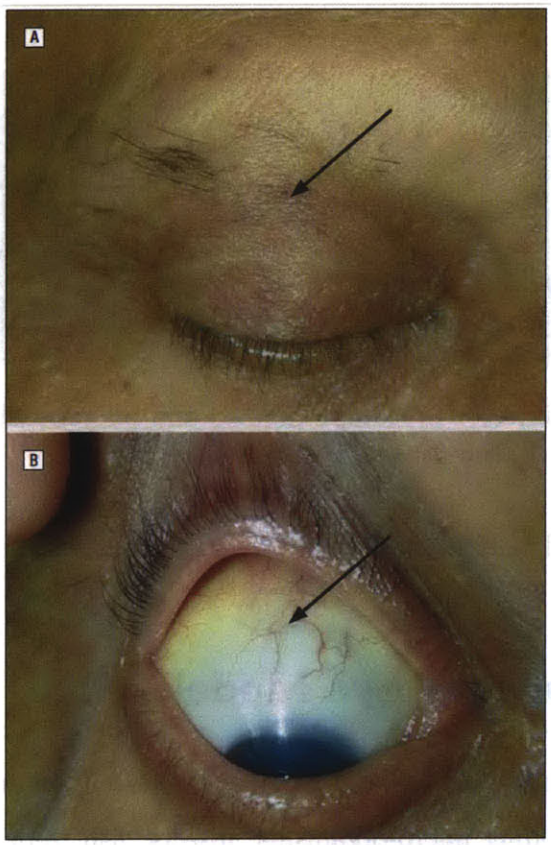

Figure 2-11: Clinical images from am accidental intravitreal Dermojet injection, taken from Y. Barak et al. [7]. (A) Small needle-like hole visible in the right brow area (arrow). (B) Episcleral veins; injection mark is visible in the upper conjunctiva surrounding the entry wound (arrow).

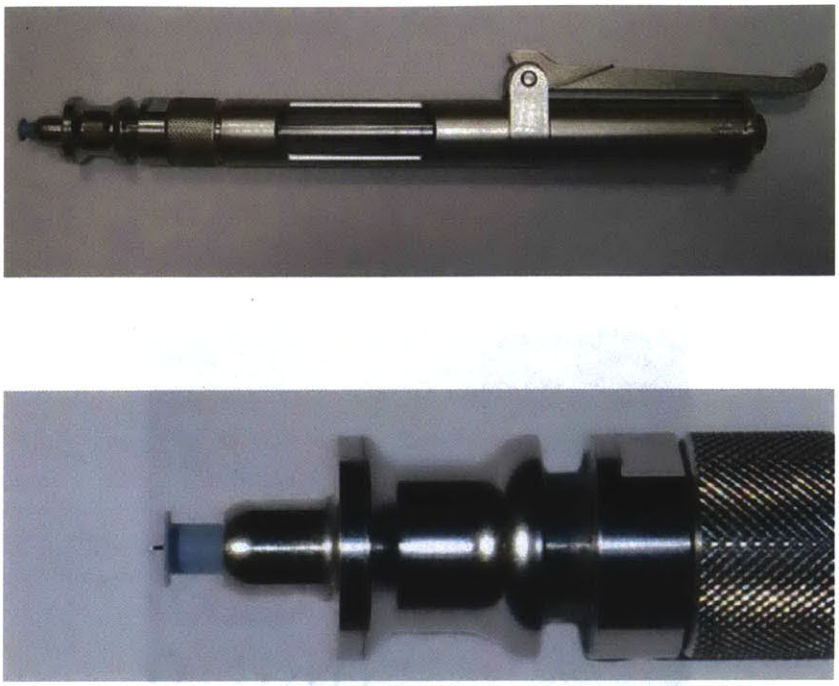

Figure 2-12: The jet injector prototype (above) and microneedle with flange (below) in magnification view, taken from G. Peyman et al. [8].

diameter needle), and needle contamination and replacement.

2.4 Experimental Eye Model

For various ocular disease models and biological research, an array of animal models are appropriate, including micro-organisms, insects, fish, reptiles, birds, and mammals [30].

For intravitreal injection studies targeted at human treatment, it is necessary to use an eye model with dimensions on the order of the human eye. Animal models commonly used for intravitreal injection studies include porcine [31], rabbit [32], primate [33], and rodent [34]. However, the response of rodent models can vary significantly from that of humans [34].

Although porcine and monkey models have anatomical structure more similar to the human eye, rabbit eyes were ultimately chosen based on availability. Mouse eyes were investigated but rejected as useful models. For the study in this thesis, the two

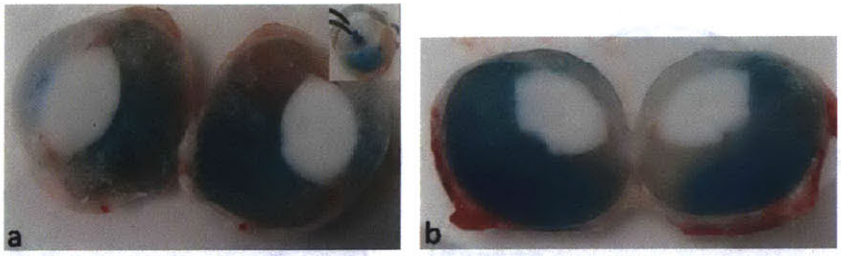

Figure 2-13: Representative cross-sections of frozen rabbit eyes following *in vivo* intravitreal injection of blue dye, taken from G. Peyman et al. [8]. (A) Microneedle-assisted jet injection (6.72 MPa). Inset shows bluish injection area. (B) Control intravitreal injection using a 412.8 µm diameter needle (27-gauge) and syringe.

	Rabbit	Man
Anteroposterior Globe Dimension (mm)	16–19	24
Cornea Horizontal Diameter (mm)	15	11.7
Lens Thickness (mm)	7.6	4
Scleral Thickness (mm)	0.2–0.75	0.3–1.0
Scleral Young's Modulus (MPa)	0.78	2.3

Table 2.1: Comparison of human and rabbit eye properties. [30] [19] [20] [35]

most relevant differences in the human and rabbit eye anatomies are the lens size (relative to globe size) and scleral properties. The lens size of the rabbit eye is larger than the human lens relative to the size of the eye [30] as shown in Fig. 2-14. The rabbit scleral stiffness is three times less than the human stiffness [35], but scleral thickness is similar [30]. Table 2.1 lists relevant values for comparison.

Synthetic eye models were considered. Using a mold and contact lens, an injection surface and vitreous humor can be simulated. Several contact lenses have properties comparable to the sclera. However, due to the immediate success of the rabbit eye as a model, the synthetic eye was not used.

2.5 Velocity Calculation Methodology

This thesis mentions four different types of velocity: potentiometer-measured coil velocity, coil volumetric-estimated jet velocity, piston-tip volumetric-estimated jet velocity, and electromechanics-estimated jet velocity.

Potentiometer-measured coil velocity is calculated from a discrete derivative of

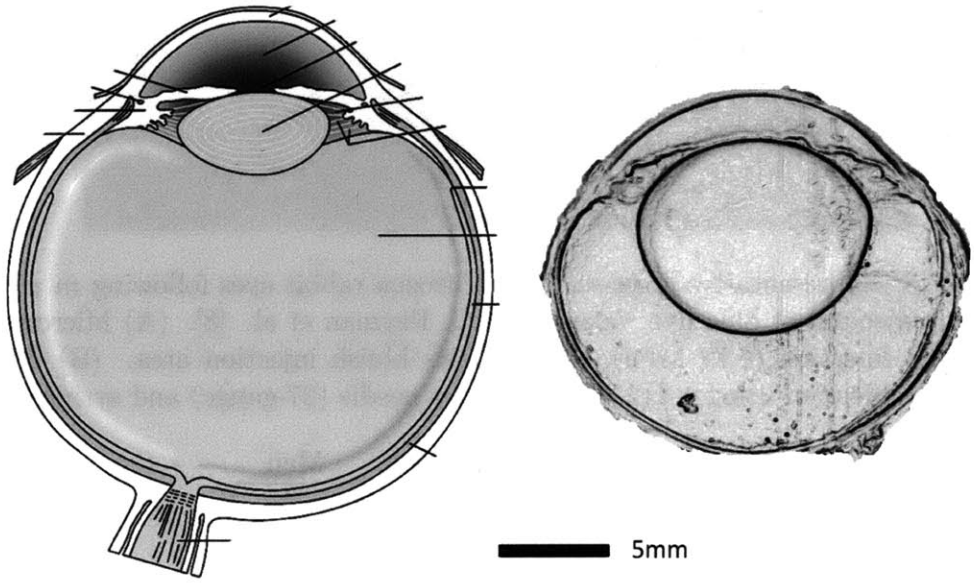

Figure 2-14: A scale diagram of the human eye (received in communications with Institut de la Vision & Sanofi-Fovea, Paris) and a post-processed cryotomed cross-section image of a rabbit eye used in this thesis. Shown in same scale.

the potentiometer-based position waveform. Position $p(i)$ is measured every step i using a relationship between the voltage output of the potentiometer system and displacement. v_{coil} at every step is then calculated as follows:

$$v_{coil}(i) = \frac{p(i) - p(i-1)}{t_{sample}}, \tag{2.1}$$

where t_{sample} is the intersample interval at which measurements were taken.

Coil volumetric-estimated jet velocity, used in the previous BioInstrumentation Lab device, is an average jet velocity calculated based on the potentiometer-measured coil velocity (v_{coil}), the diameter of the rubber piston tip (D_{piston}), and the inner nozzle diameter (D_{nozzle}). Essentially, the amount of fluid displaced by the piston flows through the nozzle, creating a jet with an average velocity calculated as follows:

$$v_{coiljet}(i) = v_{coil}\frac{D_{piston}}{D_{nozzle}}. \tag{2.2}$$

Piston-tip volumetric-estimated jet velocity uses the piston tip velocity instead of the coil velocity. The piston tip velocity is measured directly using a high-speed

camera and a pixel interpolation video processing algorithm. This method is more accurate than using coil velocity because it is closer to the piston-fluid interface and not subject to the error induced by compression of the rubber piston tip. Calculation of this velocity is as follows:

$$v_{tipjet}(i) = v_{tip}\frac{D_{piston}}{D_{nozzle}}. \tag{2.3}$$

Electromechanics-estimated jet velocity is calculated for some intravitreal injections because the high-speed camera is used to film the eye instead of the piston tip, but the coil volumetric-estimated jet velocity is too inaccurate. In this case, the jet velocity may be estimated using the electromechanical properties of the system and Bernoulli's Principle as follows:

$$v_{emjet} = \sqrt{\frac{2P}{\rho}}, \tag{2.4}$$

where v_{emjet} is the average jet velocity, ρ is the density of the fluid, and P is the pressure in the ampoule. To estimate the pressure in the ampoule, the force on the piston tip is calculated and divided by ampoule area. Piston tip force is estimated by subtracting the force used to accelerate the coil system from the Lorentz force generated by the coil. Combining these properties leads to the following calculation of the pressure:

$$P = (KI - ma_{coil})/A_{piston}, \tag{2.5}$$

where K is the motor constant, I is the peak current passing through the coil, m is the mass of the coil system, a_{coil} is the acceleration of the coil system, and A_{piston} is the area of the piston. The acceleration is approximated as constant when this method is used and estimated using the rise time (t_{rise}) and peak coil velocity (v_{peak}) as follows:

$$a_{coil} = v_{peak}/t_{rise}. \tag{2.6}$$

The peak velocity and rise time are potentiometer-measured coil velocities.

Chapter 3

JI Scleral Penetration Investigation

This chapter describes initial experiments performed to assess the effects of a high-velocity jet stream on the eye. An earlier iteration of the JI system as described in [5] was used to generate this jet stream and prove the feasibility of applying a Lorentz-force actuated JI system to IV JI.

3.1 Design

The previous electromechanical and control system was used for the first iteration of intravitreal injection testing. Eye mounts for each animal model were fabricated to allow for convenient JI IV, and control parameters were calculated for intravitreal injection in each animal model (discussed below). Four parameters were used to generate each two-phase injection waveform for the system to follow: injection jet velocity (v_{jet}), injection jet duration (t_{jet}), follow-through velocity ($v_{followthrough}$), and total desired volume ($V_{desired}$). Velocities used in this section are coil volumetric-estimated jet velocities.

3.2 Testing

Two preliminary animal models were used for this iteration: mouse and rabbit.

Figure 3-1: SolidWorks model of 3D printed eye mount for mouse eye injections. 30 mm in diameter.

3.2.1 Mouse Eye Model

Because of the immediate availability of mouse eyes, they were considered as a possible preliminary animal model. The anterior thickness of mouse sclera has been measured at 16.7 µm [36], two orders of magnitude thinner than the human sclera. Erosion depth in injections into previous mediums has been somewhat linear with velocity within an order of magnitude of the penetration velocity. Therefore, 10% of a common v_{jet} for penetrating skin (200 m/s) was used as a starting point for mouse eyes (20 m/s). If the mouse eye was injected with a proportional volume of fluid to the human eye, the amount injected would be 0.37 µL, which is too small for the original injector to deliver at a high speed. Various other values for $V_{desired}$, between 2 µL and 20 µL, were used instead.

A mount, shown in Fig. 3-1 was developed for holding seven mouse eyes in place for injection trials. The mount was designed based on the diameter of mouse eyes received, 3.7 mm, with holes 3 mm in diameter and 3D printed using Accura SI 40 resin in a Viper SI2 3D printer made by 3D Systems.

With v_{jet} of 20 m/s, mouse eyes were dyed blue on the outside as shown in Fig. 3-2, making it difficult to discern whether the eye was injected, subjected to dye diffusion, or only dyed blue superficially. No entry hole was found under microscope examination, so it was concluded that the expected 20 m/s could not pierce a mouse eye.

Velocities were increased with further injections. With $V_{desired}$ at 20 µL, v_{jet} values

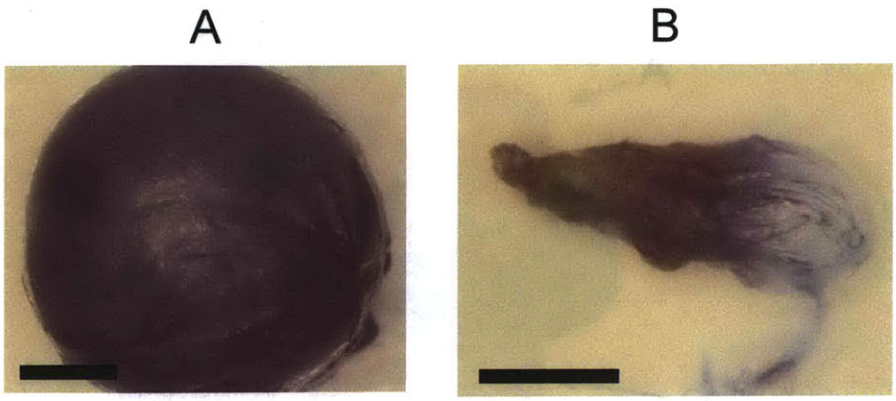

Figure 3-2: Scale bars are 1 mm. (A) Mouse eye dyed blue after 20 m/s jet injection. (B) Eye destroyed after 200 m/s 10 µL injection.

over 100 m/s were required to pierce the eyes. The waveforms for these injections were not examined, but it is likely that 100 m/s was not reached, due to 20 µL being such a small volume. Above 100 m/s, the eyes were often destroyed, as shown in Fig. 3-2. This evidence supported the hypothesis that mouse eyes were too small and delicate to be used with the previous injector. A new animal model, the rabbit, would prove useful.

3.2.2 Rabbit Eye Model

To relate the v_{jet} required to break through the sclera to the v_{jet} required to break through the skin, the pressures required by a needle to pierce the sclera and skin were calculated using the piercing force required divided by the surface area of the needle head. The contact surface area of needles were estimated using nominal outer and inner diameters. Using the force required by a 311.2 µm needle (30-gauge) to puncture the human sclera [16], an approximate sclera piercing pressure of 1.02 MPa was calculated. Using the force required by a PS-2 needle to pierce abdominal tissue, a skin piercing pressure of 0.6 MPa was calculated. However, because the human sclera is three times stiffer than the rabbit sclera, it was estimated that approximately half of skin-piercing pressure was sufficient to pierce rabbit sclera, 0.34 MPa. Because pressure is proportional to velocity squared in Bernoulli's Principle [37], and a typical skin-piercing v_{jet} is 200 m/s, a setting of 150 m/s (approximately $\frac{200\,\mathrm{m/s}}{\sqrt{2}}$) was selected

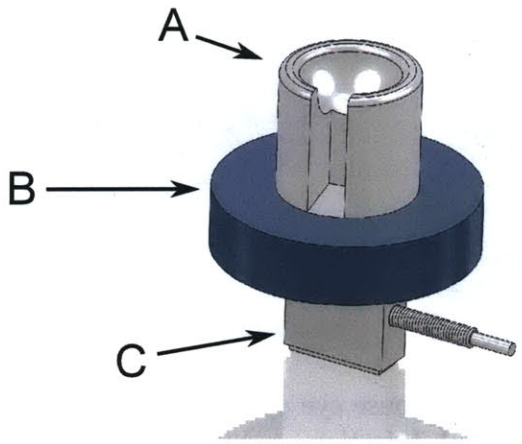

Figure 3-3: SolidWorks assembly of (A) eye fixture, (B) base, and (C) FUTEK [9] load cell. Diameter of base is 42 mm.

for v_{jet}.

An inverse dome for holding rabbit eyes was modeled, 3D printed, and fitted to a turned base of plastic. The stage was rotatable and could be fixed to a load cell as shown in Fig. 3-3. The slit through half of the eye holder allowed eye fluid to flow down the holder and acted as a window for a high speed camera to see through the pupil unobstructed. Load cell measurement was added to the data acquisition system to assess any effect load had on the injections.

The eyes were injected 2 mm posterior to the limbus. This dimension is 1 mm shorter than in humans due to the larger cornea of the rabbit. Parameters 150 m/s v_{jet}, 20 ms t_{jet}, 50 m/s $v_{followthrough}$, and 40 µL $V_{desired}$ resulted in injection. Three more eye injections were carried out with varying parameters. t_{jet} of 5 ms was not sufficient to pierce the sclera, most likely because the jet injector did not reach peak velocity in this short time. However, with a 200 m/s v_{jet} and a 10 ms t_{jet}, eye penetration was successful. As in needle injections, dye entering the eye was clearly visible through the pupil. These eyes were frozen, sectioned temporally along the axis of the injection, and examined. A representative photo of an injected eye is shown in Fig. 3-4.

Preliminary high-speed imaging was attempted using a high-speed camera (Vision Research Phantom v9.0, Wayne, New Jersey [38]). Various lighting arrangements

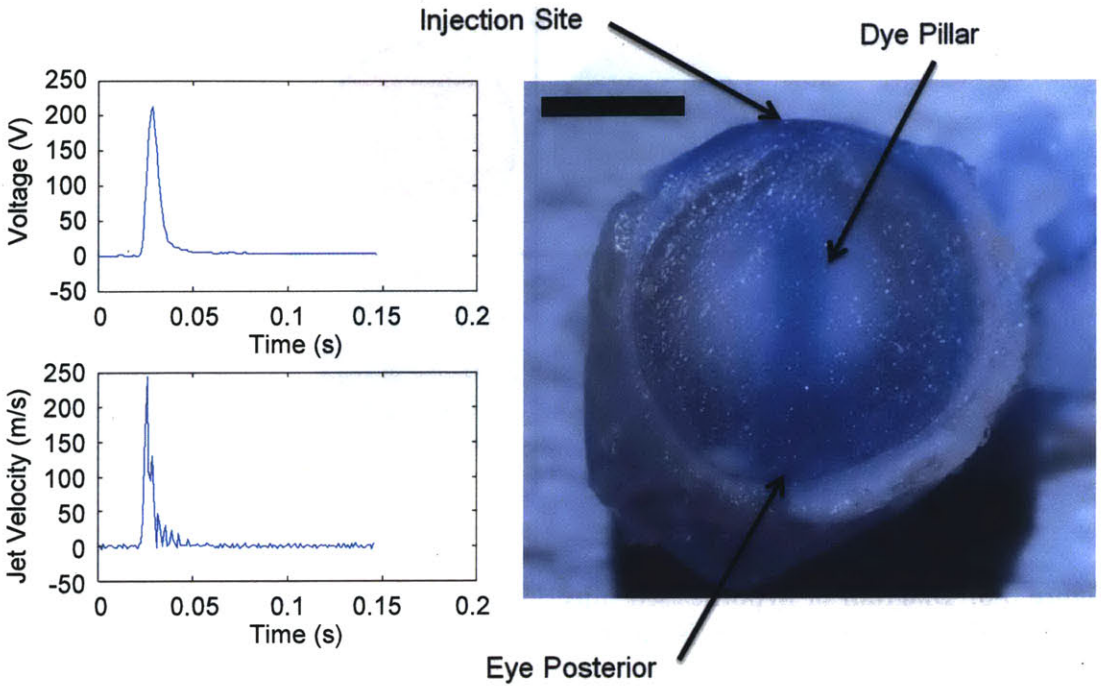

Figure 3-4: Coil voltage, jet velocity, and cross-section of rabbit eye injection. Scale bar is 5 mm.

were unsuccessful; however, a backlit set-up was promising and offered a limited view of the injection pillar forming. This method would be refined in later injections. All in all, the rabbit model was comfortable to work with and was chosen as the animal model for the next set of experiments.

3.3 Conclusions

Experimenting with the original jet injector gave insights that would define the design for the rest of the project. The injections required a similar velocity to that of skin in order to pierce the sclera. However, the vitreous and retina are soft and fragile. This led to the predicted relationship shown in Fig. 3-5. The hypothesis was that a high-velocity jet for a short amount of time may be able to pierce the sclera but not contain enough momentum to damage the eye. Additionally, $v_{followthrough}$ must be high enough to maintain the entry hole created by the jet, but low enough to prevent damage.

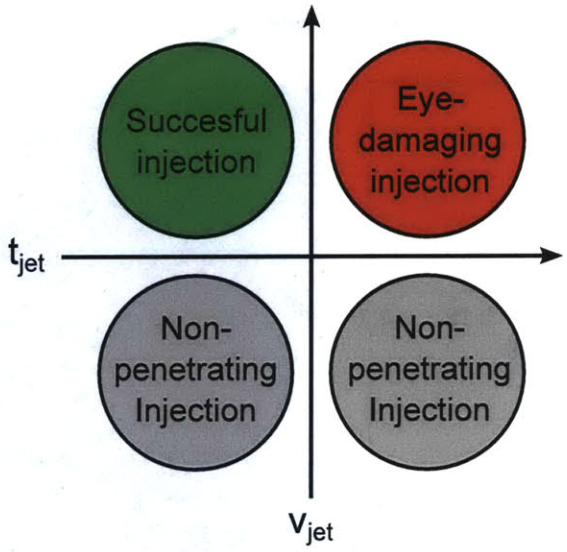

Figure 3-5: Diagram of hypothesised injection result-jet time-jet speed relationship. A short, high-velocity injection is ideal.

Directly enucleating the vitreous of the eye was unproductive, as the eye lost shape quickly. Slow freezing left ice crystals that could be eliminated by quick freezing. Cryotoming would be necessary for clear images.

The original device controller was most likely unable to follow velocity fast enough to pierce but not damage the eye. A controller based on jet velocity as opposed to jet position was hypothesized to perform better for this application.

Chapter 4

Development of a Needle-Free Intravitreal Injection Device

This chapter describes the development and testing of new control schemes that use the linear Lorentz-force actuator for needle-free intravitreal injection. Two control schemes were investigated: a bang-PD velocity controller, and a piston-tip estimation feed-forward controller.

4.1 Device Requirements

The goal of a new device in this space is to eliminate disadvantages discussed in Section 2.1 without adding risk or losing capabilities. This new system targets a number of disadvantages that can be eliminated using jet injection technology:

1. Risk of injuring eye mechanically with needle
2. Risk of infection
3. Discomfort and anxiety
4. Creation of sharps waste
5. Requirement of time from ophthalmologist
6. Inability to deliver high concentrations to the posterior region of the eye

A list of reasonable design goals were developed, preserving the functionality of the current intravitreal injection process and targeting the previously mentioned disadvantages (listed in parenthesis):

1. Doesn't require insertion of foreign object into the sclera or vitreous (1)(2)(3)
2. Creates injection hole smaller than current needles (3)
3. Completes injection procedure faster than needle injection (3)(5)
4. Doesn't require sharps (4)
5. Adds depth-targeting functionality to inject to the posterior region of the eye (6)
6. Doesn't damage eye structures, notably the lens, retina, choroid, and sclera
7. Doesn't significantly reduce efficacy of injected drug
8. Accurately injects desired drug volumes into the vitreous humor

Many similar requirements have already been fulfilled for intradermal, subcutaneous, and intramuscular injections using JI technology, but adapting the technology to the eye is an interesting challenge.

4.2 Bang-PD Velocity-Controlled System

The first iteration of the new device retained most hardware features of the original jet injector system. However, a very different two-phase controller was created, better suited to the challenge of intravitreal injection.

4.2.1 Design

The system utilized the same Injex^{TM} injection ampoules (INJEX Pharma Ltd. [39]) with jet orifices averaging 221 µm in diameter and reused the eye base stage shown in Fig. 3-3. Several hardware components of the previous system were replaced for the new system, but none of these changed the system's basic functionality. A pair

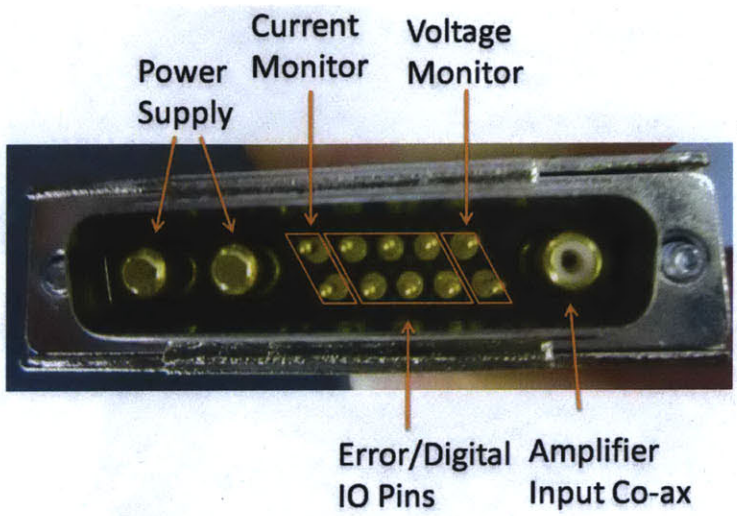

Figure 4-1: Custom-made injection amplifier connector. Width of connector is 52 mm.

of power amplifiers (AE Techron 7224 [40]) in series were used to generate the high-bandwidth voltage to control the coil. A similar FPGA and real-time interface (National Instruments cRIO-9024 [41]) were used for device control, camera triggering, and user input.

A control panel and vertical positioning stage were added to make the benchtop device easy to test. An amplifier interface, shown in Fig. 4-1, was custom-developed for the new system to allow the amplifier to be conveniently connected and disconnected from an injection device and reduce noise. A precision voltage reference (Texas Instruments REF102 [42]) was added to increase the signal-to-noise ratio of the potentiometer position measurement. A high-speed camera (Vision Research Phantom v9.0 [38]) was mounted facing perpendicular to the path of injection with a macro lens to obtain intraocular video through the pupil. When triggered from the FPGA, the camera records at 6400 fps at a resolution of 192 $\times$ 192 pixels. Lighting was provided by a 150 watt source (Dolan-Jenner Fiber-Lite A3200 [43]), front- and back-lighting the eye. A photo of the complete intravitreal injection and analysis system is shown in Fig. 4-2. A photo of the eye staging area of the intravitreal injection system is shown in Fig. 4-3.

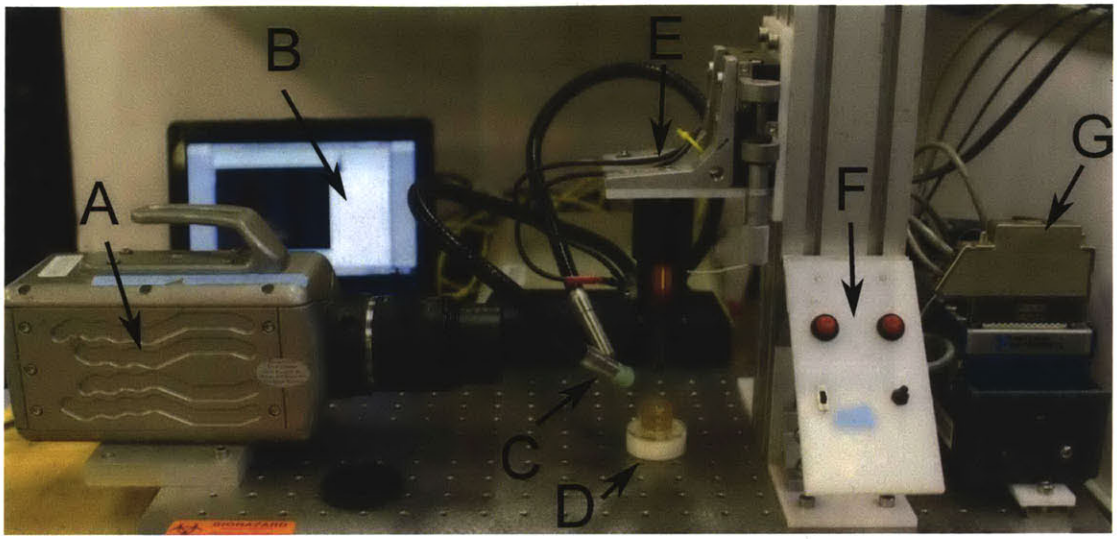

Figure 4-2: Complete benchtop intravitreal injection system. (A) High-speed camera. (B) Camera control software on laptop. (C) High-intensity lighting. (D) Rabbit eye positioning stage. (E) JI injector on vertical stage. (F) Control panel. (G) FPGA and real-time control and data acquisition device.

The control scheme used in an earlier version of the jet injector was replaced to facilitate IV JI. The speed and duration of an injection jet as discussed are key factors in penetration depth [5], which is essential for successful IV injection. In an IV JI, the jet speed must be high enough to pierce the sclera [16], yet the jet duration must be short enough to not damage the retina. To estimate the coil velocity, a discrete derivative of the 100 kHz-sampled coil position was smoothed by a 10 kHz Butterworth low-pass filter.

In the control scheme, an initial bang controller (rising phase of a bang-bang controller) was used to reach a high coil velocity in minimum time. This stage was followed by proportional-derivative (PD) control of velocity to a preset follow-through velocity. Within 5% of the preset coil position (proportional to injection volume), the controller transitioned into PD position control. PD control gain values were initially set based on previously performed system identification and later tuned by ejections of water into air. The controller can be represented by the block diagram or pseudocode in Fig. 4-4. Three parameters were used to generate each two-phase injection waveform for the system to follow: bang injection jet velocity (v_{bang}), follow-through

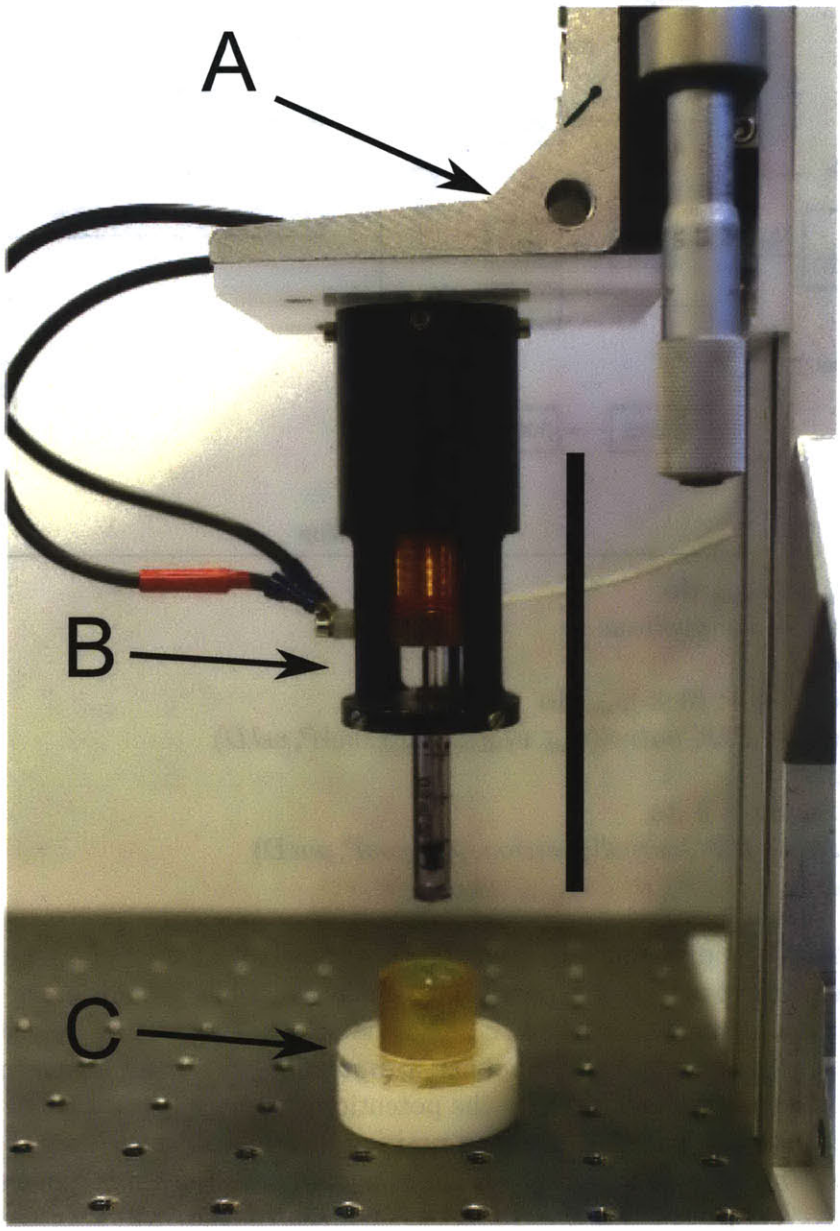

Figure 4-3: IV jet injector. Scale bar is 100 mm. (A) Injector height adjustment stage. (B) Lorentz-force actuated jet injector. (C) 3D-printed artificial orbit for eye mechanical support and positioning.

velocity ($v_{followthrough}$), and total desired volume ($V_{desired}$). The coil position corresponding to the desired delivery volume, p_{set}, is calculated using the potentiometer displacement relationship.

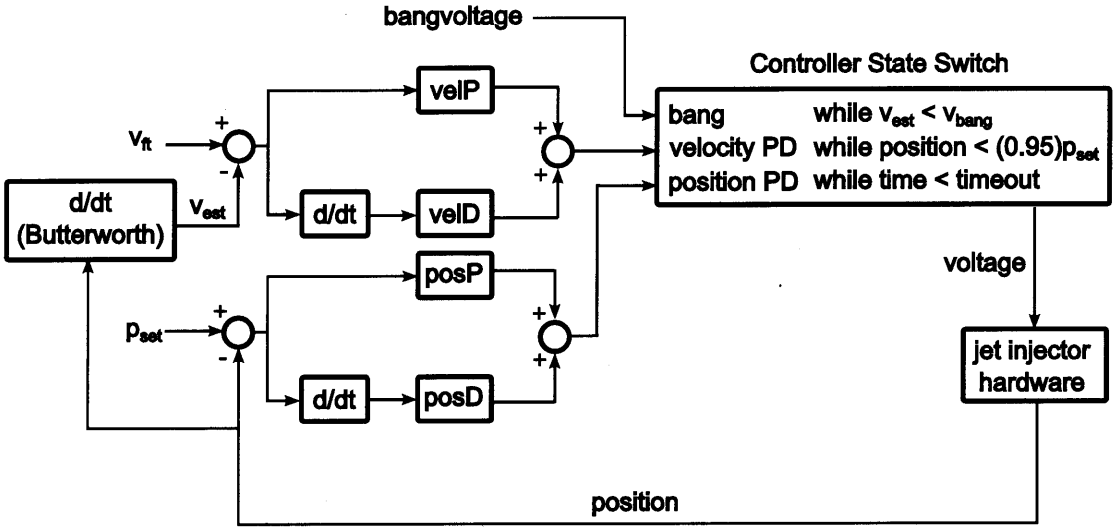

while $v_{est} < v_{bang}$ **do**
  $voltage \leftarrow bangvoltage$
end while
while $position < (0.95)p_{set}$ **do**
  $voltage \leftarrow PDControl(v_{est}, v_{followthrough}, velP, velD)$
end while
while $timeout > 0$ **do**
  $voltage \leftarrow PDControl(position, p_{set}, posP, posD)$
end while

Figure 4-4: Block diagram and pseudocode of control algorithm. The controller state switch progresses to the next state when the 'while' condition is false. v_{est} is the real-time estimated velocity, v_{bang} is the set bang controller velocity, *voltage* is the voltage command to the amplifier, *bangvoltage* is a bang control parameter, *position* is the position measured by the potentiometer, $v_{followthrough}$ is the set follow-through velocity, p_{set} is the set injection position, $velP$, $velD$, $posP$, $posD$ are control parameters, *time* increases throughout the injection, and *timeout* is a preset injection time limit.

Although v_{bang} and $v_{followthrough}$ settings for the control system are stated as potentiometer-measured coil velocities, it is useful to estimate the average velocity of the fluid jet. Potentiometer-measured coil velocities agreed well with the low piston-tip volumetric-estimated jet velocities of the follow-through phase of the controller. However, during the bang phase of the controller, the fast system dynamics resulted

in a large error between camera-measured and volumetric-estimated jet velocity. Because the high-speed camera was directed at the pupil during IV JI instead of the piston tip, electromechanics-estimated jet velocity as mentioned in Section 2.5 was used to characterize the peak velocity of the injection. Compared with high-speed piston tip camera video, electromechanics-estimated jet velocities exhibited a peak velocity RMS error of 7.8 m/s.

4.2.2 Bang-PD Velocity Controller Testing

The controller improved the velocity profile for low-duration high-velocity JI. From rest, the bang controller reached coil velocities of 2.5 m/s within 1.5 ms, and the PD velocity controller slowed the coil to the follow-through velocity within 1 ms, shown in Fig. 4-5. The high-velocity segment of the injection lasted less than 2 ms, about half the duration of the earlier controller's high-velocity jet. The PD position controller activated when the position was within 5% of the set-point. The controller held the set-point until the injection time was reached.

Bang control of the injector system overshot the target velocity, as shown in Fig. 4-5, due to the controller lag and third-order Lorentz-force actuator system dynamics. When switching to the follow-through velocity segment, the PD controller undershot the set velocity, even reversing direction. Tuning the PD controller to undershoot ensured that fall time was short, which is critical to minimize tissue destruction, and the real jet velocity never dropped below zero (verified by high-speed camera). The overshoot and undershoot were not repeatable, most likely due to the time-varying dynamics of the system (i.e., ampoule degradation) and varying injection initial conditions (i.e., initial compression or relaxation of piston tip). During the follow-through phase the system exhibited periodic oscillations, possibly due to non-linear friction of the ampoule.

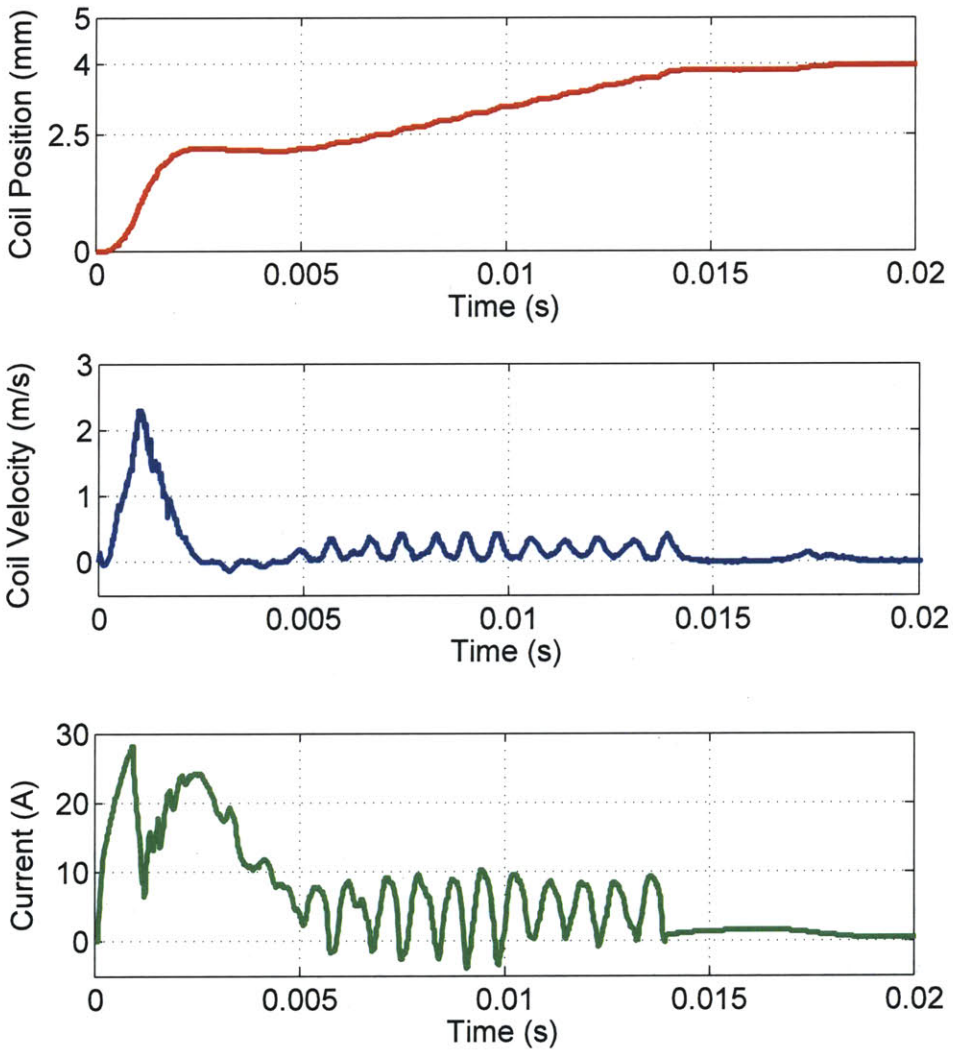

Figure 4-5: Representative injection results with bang-PD velocity controller. Set parameters: 2.5 m/s coil bang velocity; 0.2 m/s coil follow velocity; 40 µL delivery volume (4 mm set-point).

4.2.3 Rabbit Eye Injection Testing

Nine rabbit eyes were obtained through the MIT Tissue Harvest Program using procedures approved by the MIT Committee on Animal Care and in accordance with the NIH Guide for the Use and Care of Laboratory Animals. Explanted eyes were refrigerated in saline solution for no more than 4 hours before the injection trial. In each trial, 40 µL of 0.25% bromophenol blue dye solution was injected 3 mm from the *limbus corneae* at the *pars plana*, the recommended site for human IV injection [25]. A 3 mm distance from the *limbus corneae* was chosen for this trial because, although the cornea of the rabbit is large, its *pars plana* is also farther posterior. Settings for v_{bang} ranged from 2.04 m/s to 2.42 m/s and settings for $v_{followthrough}$ ranged from 0.05 m/s to 0.20 m/s.

Immediately after injection, eyes were embedded in optimal cutting temperature compound (Tissue-Tek O.C.T. Compound 4583, Torrance, CA) in liquid nitrogen. The samples were wrapped in foil and stored at -20 °C until needed. The resulting O.C.T.-eye blocks were sectioned and imaged in 30 µm increments superior and perpendicular to the axis of injection using a cryostat vibratome (GMI Inc. Vibratome UltraPro 5000, Ramsey, MN).

A typical injection time-line is shown in Fig. 4-6. No vitreal reflux was observed after any injection, but sectioning revealed that 7 out of 9 eyes exhibited retinal tearing. To numerically characterize the post-injection eye results, two metrics were defined: retinal tear diameter and entry hole diameter. These metrics were measured as shown in Fig. 4-7. Electromechanics-estimated jet velocity is used to describe the peak jet velocity of each rabbit eye injection. Two injections resulted in no retinal tearing, as shown in Fig. 4-8, and had peak jet velocities of less than 171 m/s and follow-through velocities of less than 6.8 m/s.

To relate velocity profile characteristics to eye damage metrics, the peak velocity and average follow-though velocity of each injection were recorded. Next, to isolate the effects of each velocity, the data was divided into two groups: five injections with similar peak velocities (161 m/s ± 8 m/s) and four injections with similar follow-

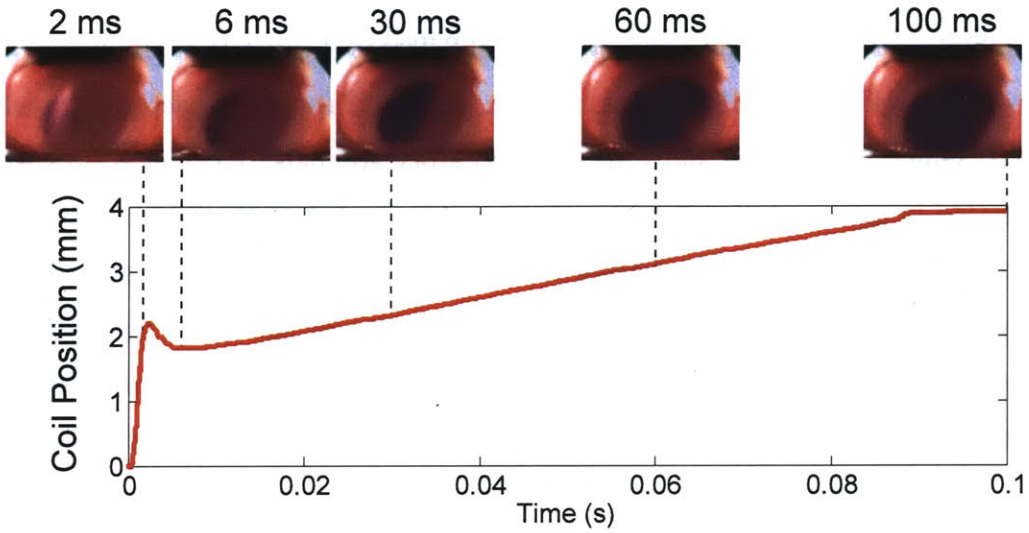

Figure 4-6: Timeline of injection, showing high-speed camera images and velocity profile. Peak jet velocity: 170 m/s; average follow-through velocity: 6.7 m/s. Eye exhibited no retinal tearing.

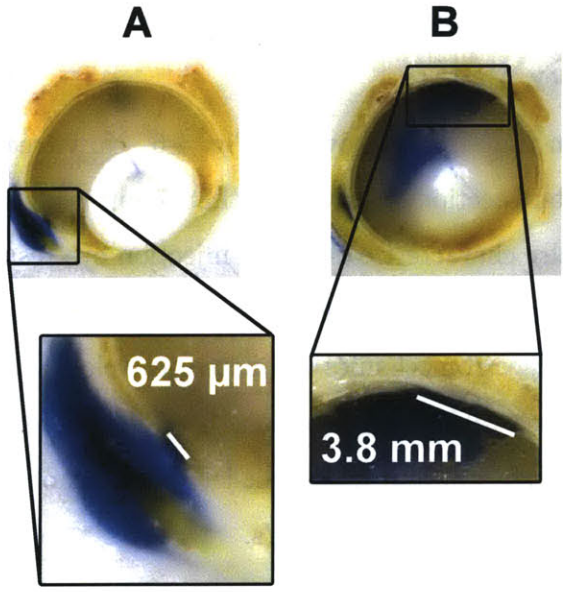

Figure 4-7: Injection result measurement methodology. (A) Entry hole diameter is measured as the largest width of choroid puncture in sections. (B) Retinal tear diameter is measured as the largest width of detached retina in sections.

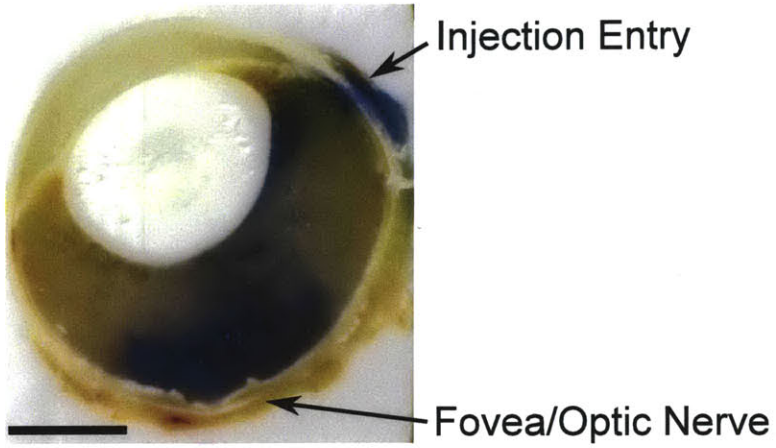

Figure 4-8: IV JI exhibiting no retinal tearing. Scale bar is 5 mm. (Superior view of cross-section, showing injection site and target.)

through velocities (6.45 m/s ± 0.41 m/s). Remaining eye injection results were not used for analysis. For each isolation group, the jet velocities were plotted against both eye damage metrics, shown in Fig. 4-9. The plots show a positive correlation between tissue damage and increasing velocities. The results suggest that for some follow-through jet velocity between 6.58 m/s and 28.9 m/s the follow-through phase begins to cause retinal tearing. Likewise, for some peak velocity between 170 m/s and 201 m/s, the peak velocity jet begins to cause retinal tearing.

4.2.4 3D Injection Reconstruction

Penetrating depth, dispersion, and an estimate of the volume of drug delivered to the eye can be calculated by reconstruction of a 3D model of the injected eye from 2D slices of the eye. This was accomplished with 30 µm section images of the injected eyes, taken using a 50 mm compact-macro lens while being sectioned on a cryotome. Custom image recognition software was developed in MATLAB® [44] to automatically differentiate between eye tissues and injection dye in these sections using hue-saturation-value ranges, a process shown in Fig. 4-10. Once these structures were recognized on every eye section, the software reconstructed the features into a 3D representation of the injection result, shown in Fig. 4-11.

These 3D data can also give us insight as to where the injected fluid has highest

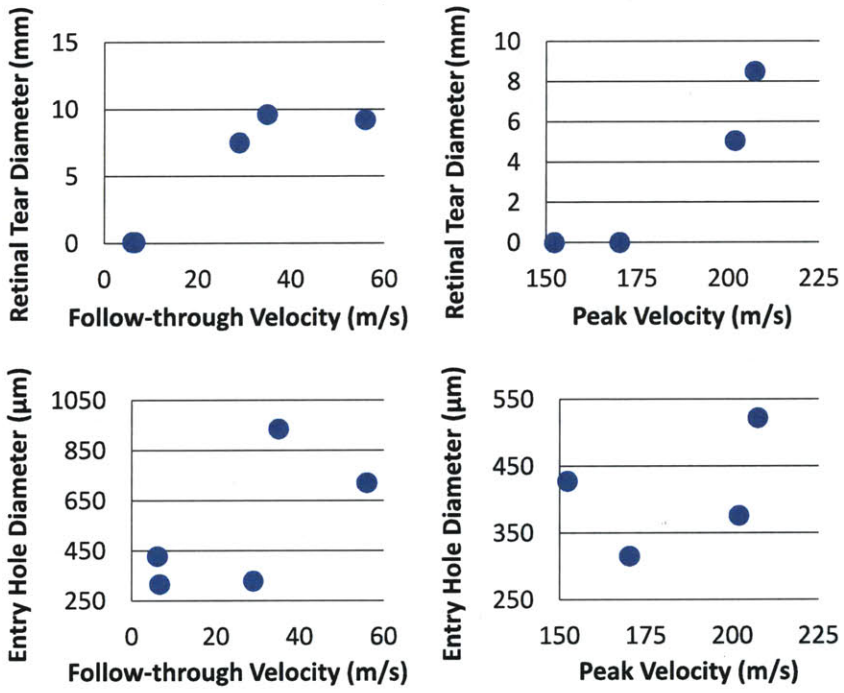

Figure 4-9: Plots of two velocity profile characteristics vs. two eye damage metrics. For varying follow-through velocities, the peak velocity is 161 m/s $\pm$ 8 m/s; for varying peak velocities, the follow-through velocity is 6.45 m/s $\pm$ 0.41 m/s.

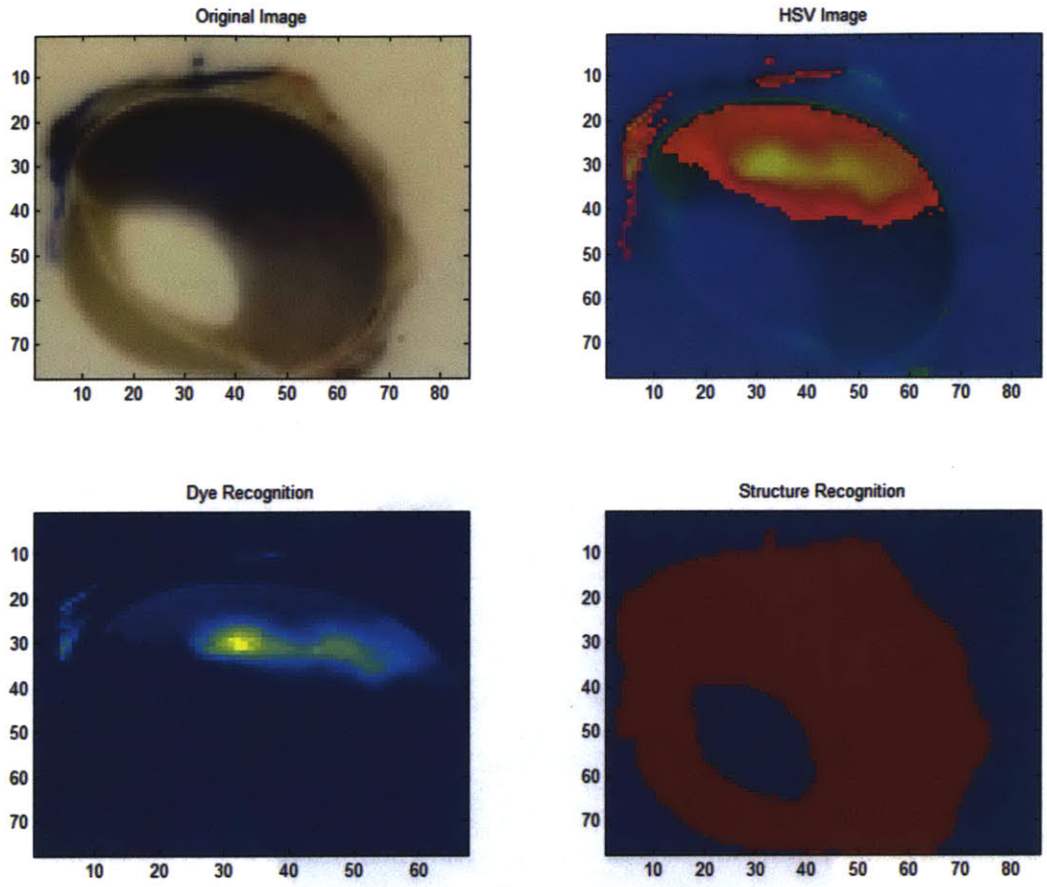

Figure 4-10: Image recognition process visualized on one 30 µm section of eye. Axis shown are in pixels (10 pixels is approximately 3.2 mm. (Top-left) Raw image of sectioned eye. (Top-right) red-green-blue image visualization after being converted to hue-saturation-value color representation. (Bottom-left) Region of image recognized as blue dye. (Bottom-right) Region of image recognized as eye structure.

concentration. This is most useful within the vitreous, where the visual properties of the dye are most uniform. Challenges still exist, such as accounting for the dye appearing darker in the sclera than it does in the vitreous, due to natural tissue pigment. Also, in Fig. 4-11 the effects of imperfectly aligned sectioning can be seen where the inside of the eye structure exhibits ridges. The visual 3D reconstruction technique is not an exact tool yet, but it allows us to visualize and analyze the data in an entire new dimension. For example, in Fig. 4-11, it is clear that dye travelled to and stopped at the target site at the back of the eye.

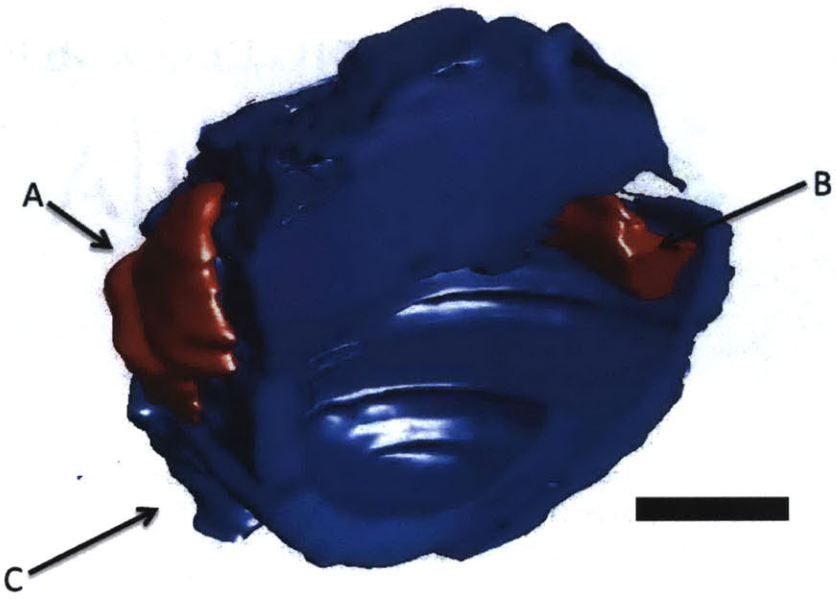

Figure 4-11: Reconstructed eye structure (blue) and dye (red). Scale bar is 5 mm. (A) Dye around entry site. (B) Dye at target site. (C) Structures recognized as eye tissue.

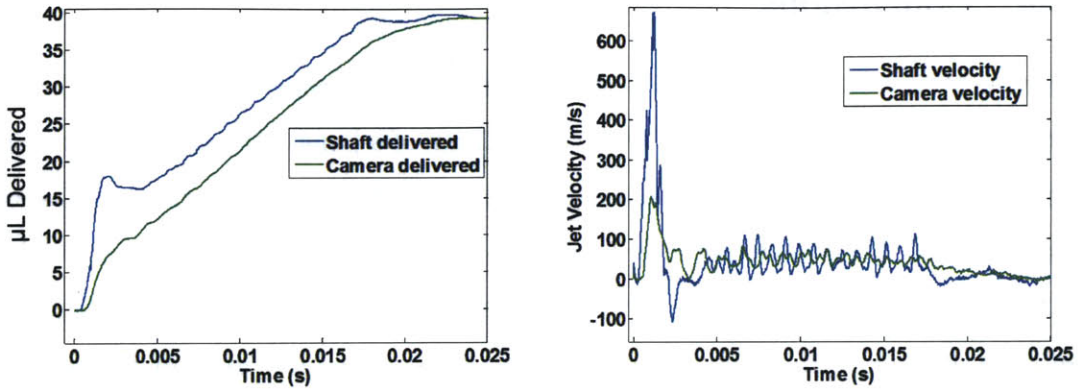

Figure 4-12: Comparison of the volumetrically estimated volume delivered (left) and volumetrically estimated jet speed (right) from the shaft potentiometer (blue) and the piston tip high-speed camera (green).

4.2.5 Dynamics-Induced Jet Speed Error

The compression of the piston tip during an injection is substantial. Earlier tests of the device have also shown that the ampoule itself strains noticeably. Together, these two dynamic elements make the volumetric estimations from the coil position very error prone, especially for the short, high-velocity jets that need to be achieved in IV JI.

To measure the piston tip-induced error, the high speed camera recorded video at 51,282 fps while pointed at the piston tip during an ejection of water into air. After injection, custom video processing software was used to calculate the piston tip position in each frame. Displacement resolution similar to the potentiometer displacement resolution was reached by interpolating the distance travelled between the center of pixels. The resulting volumetric estimation comparisons showed that the coil peak velocity measurement can overestimate the piston tip peak velocity by more than 300%. Equally important, the piston tip spends a prolonged period at high velocity due to the feedback loop that maintains a steady shaft velocity. A sample comparison of the coil-measured and piston tip-measured values is shown in Fig. 4-12. To combat the adverse effect this phenomenon has on the eye interface jet speed, a new controller was needed.

4.2.6 Conclusions

These injections showed that IV JI can be accomplished using a pre-existing linear Lorentz-force actuated jet injector with the addition of a bang-PD velocity controller. As predicted, Fig. 4-9 indicates that low peak and follow-through velocities reduce retinal tearing. Entry hole diameter is also positively correlated with both velocities but exhibits a higher deviation between injections. Four eyes had entry hole diameters less than 400 µm, within the range of needle sizes commonly used in intravitreal injections. This is important, as pain and drug reflux have been shown to increase with larger needles [17] and may similarly increase with larger IV JI entry holes. Moreover, the IV JI duration is less than 100 ms, minimizing patient discomfort and procedure time.

Eye sections with and without retinal tearing suggest that IV JI can target the fovea and optic nerve, as shown by the dye concentration in Fig. 4-8. In a needle injection, delivery to this area relies on convection and diffusion, but much of the drug will be transported to areas other than the target, as shown in Fig. 2-4. Higher concentrations of drug near the target site are favorable because they reduce the total amount of drug needed, therefore reducing the effect of the drug on non-target areas [45].

4.3 Piston Tip Estimation Feed-Forward System

The goals of this iteration were to improve controller performance and post-IV JI analysis. The previous iteration suggested that better controller performance (i.e. more accurate following of high-velocity short-duration jets) leads to more repeatable, less damaging injections.

4.3.1 Design

As shown in Fig. 4-12, substantial piston compression caused a large error between coil position and piston tip position. To control the position of the piston tip, a coil-

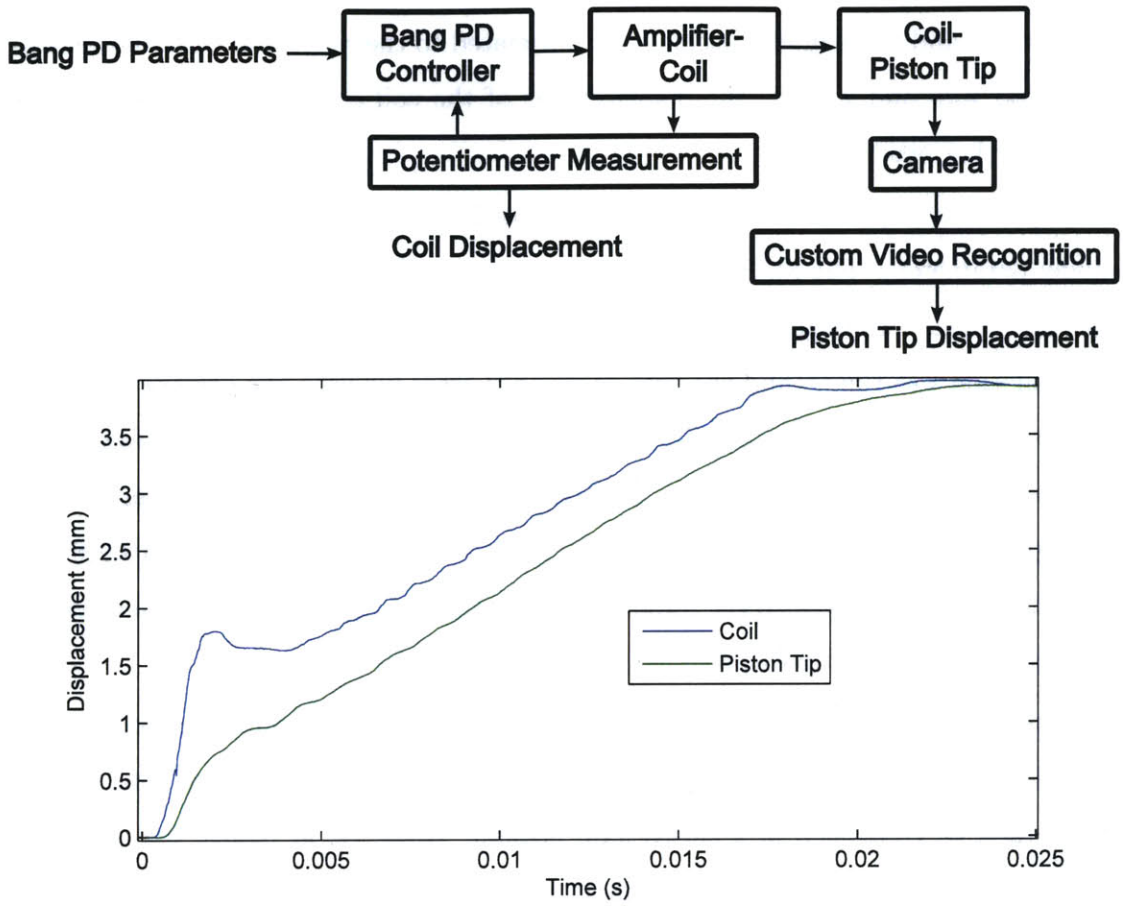

Figure 4-13: Measuring method for transfer function development.

tip transfer function was required. The data acquisition set-up from Section 4.2.5 was used to record data for developing a transfer function. The previous bang-PD controller was used to generate the waveforms used for analysis. As shown in Fig. 4-13, this resulted in two time-dependent waveforms, coil displacement and piston tip displacement by which to fit a transfer function for the system.

It was determined with sensitivity analysis that a 2nd-order linear model relating coil displacement and piston tip displacement, coupled with a piston tip damping term, was sufficient for predicting the motion of the system. This model was represented by the following differential equation:

$$\ddot{x}_{tip} = m(x_{coil} - x_{tip}) + b(\dot{x}_{coil} - \dot{x}_{tip}) + k|\dot{x}_{tip}|\dot{x}_{tip}, \tag{4.1}$$

where m, b, and k are model parameters (unrelated to their classical dynamics meanings) and x_{coil} and x_{tip} are the displacement of the coil and tip, respectively, from their starting positions.

An iterative optimization process, shown in Fig. 4-14, was used to calculate the model parameters. The MATLAB® function *lsqcurvefit* was used as a fast algorithm for this process. To begin the process, three parameters (m, b, and k) were guessed. A simulation was run to find the sum of squared error between the camera measured tip displacement and the simulation tip displacement. The previous guesses were then refined in trust-region-based optimization to minimize the sum of squared error. This guess-check repeated until the change in error was below a threshold (0.0001%). Sensitivity analysis revealed the importance of each transfer function term in correctly predicting the piston tip displacement, shown in Fig. 4-15.

Theoretically, the position of the coil throughout a real-time injection can be transformed by the model to predict the piston tip position. This real-time system could then be controlled in a closed-loop fashion. However, in reality the necessary calculations to update the system estimation created significant lag and required more gates than available on the controller FPGA. For this reason, it was decided to pre-generate a coil state waveform that, when used to simulate piston tip state, results in a desired piston tip waveform. Using a controller with high gain, a simulated injection was run in which the coil displacement was controlled so that the simulated tip displacement followed the desired tip displacement, as shown in Fig. 4-16. The desired tip displacement waveform was created using the same four parameters as the original system: injection jet velocity (v_{jet}), injection jet duration (t_{jet}), follow-through velocity ($v_{followthrough}$), and total desired volume ($V_{desired}$).

The results of the simulation were used to generate a full state feed-forward waveform to achieve desired piston tip displacement. A compensation command was created based on desired coil acceleration, damping from coil friction, and piston tip compression forces. Position and velocity waveform control corrected for error during the injection. An example of the final waveforms used by FPGA control is shown in Fig. 4-17.

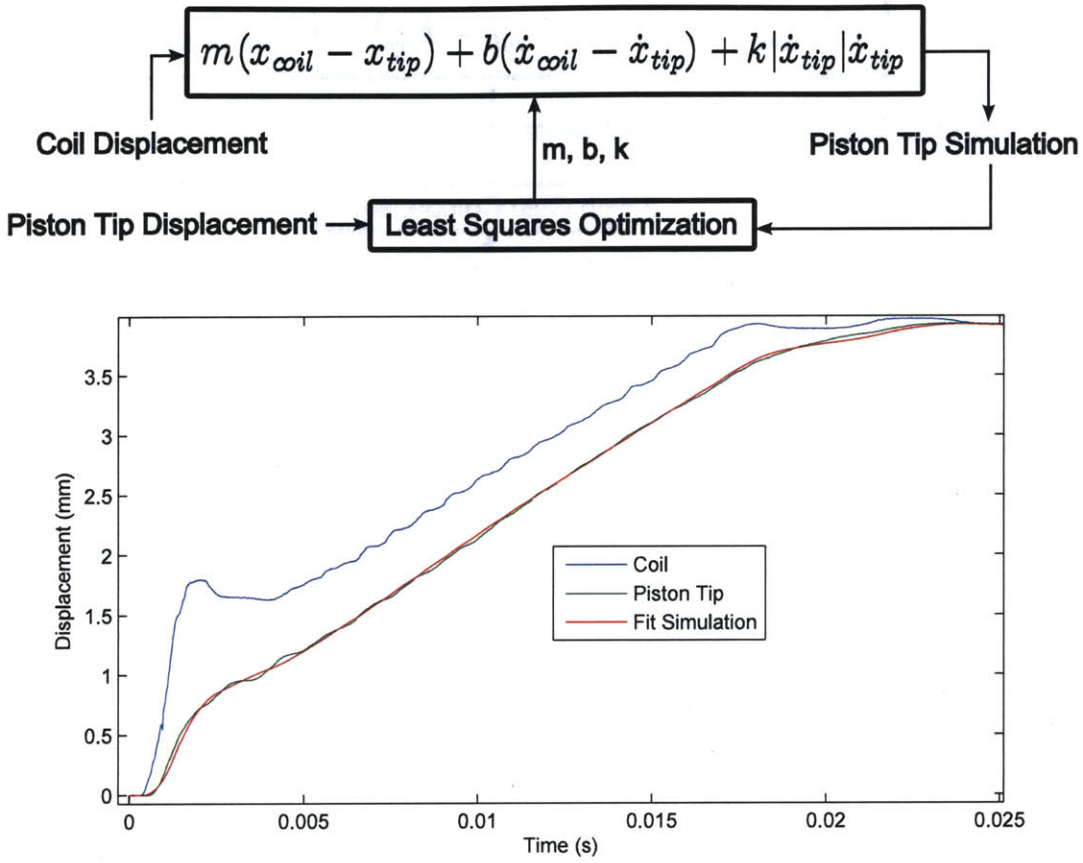

Figure 4-14: Method of determining coefficients for the coil displacement to tip displacement transfer function.

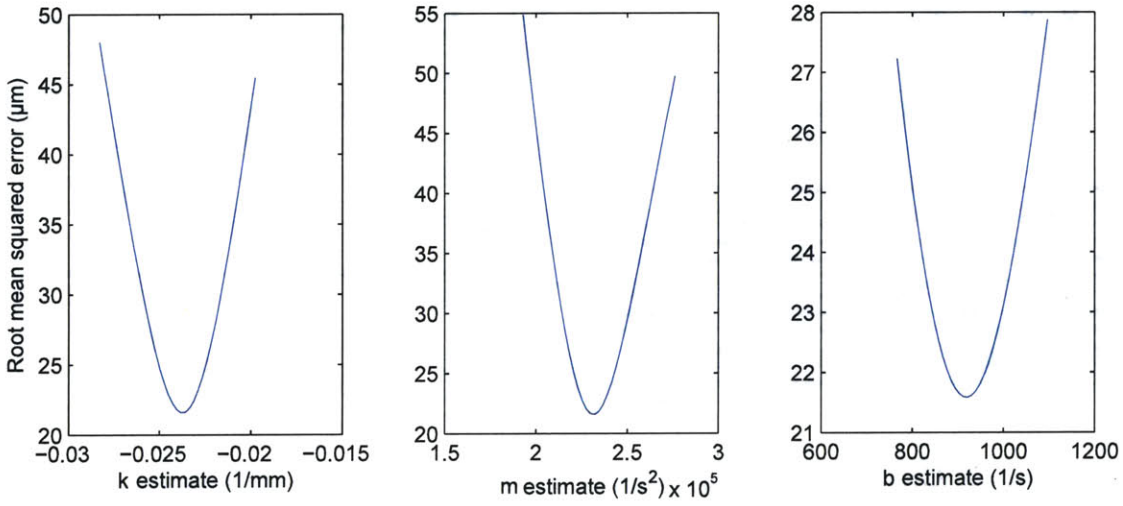

Figure 4-15: Sensitivity analysis around the optimization result for each transfer function term coefficient.

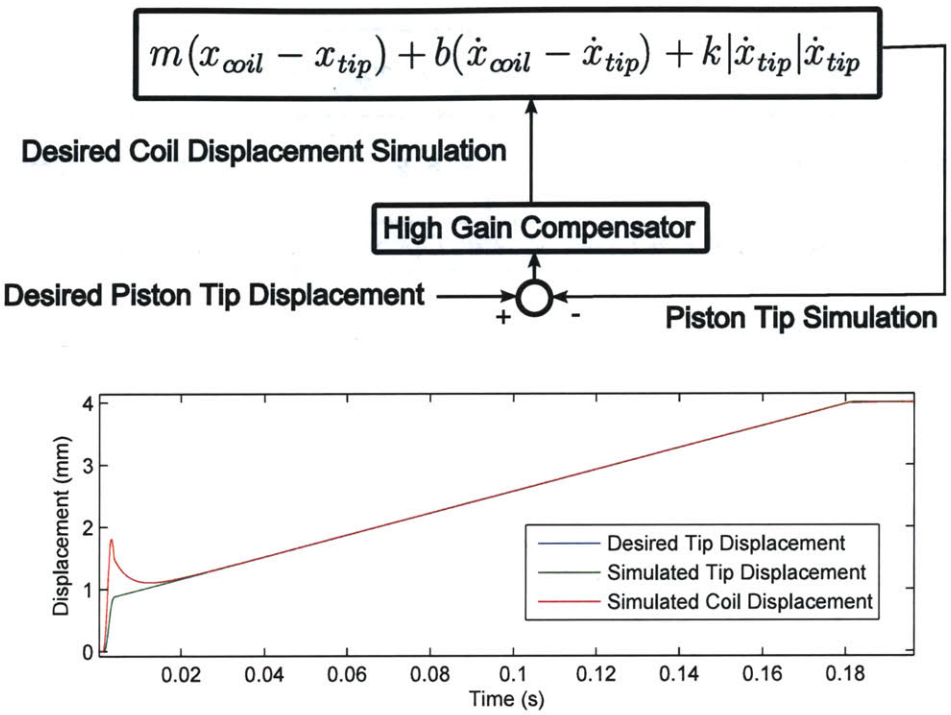

Figure 4-16: Block diagram and graph of simulation control for developing a desired coil displacement from a desired tip displacement.

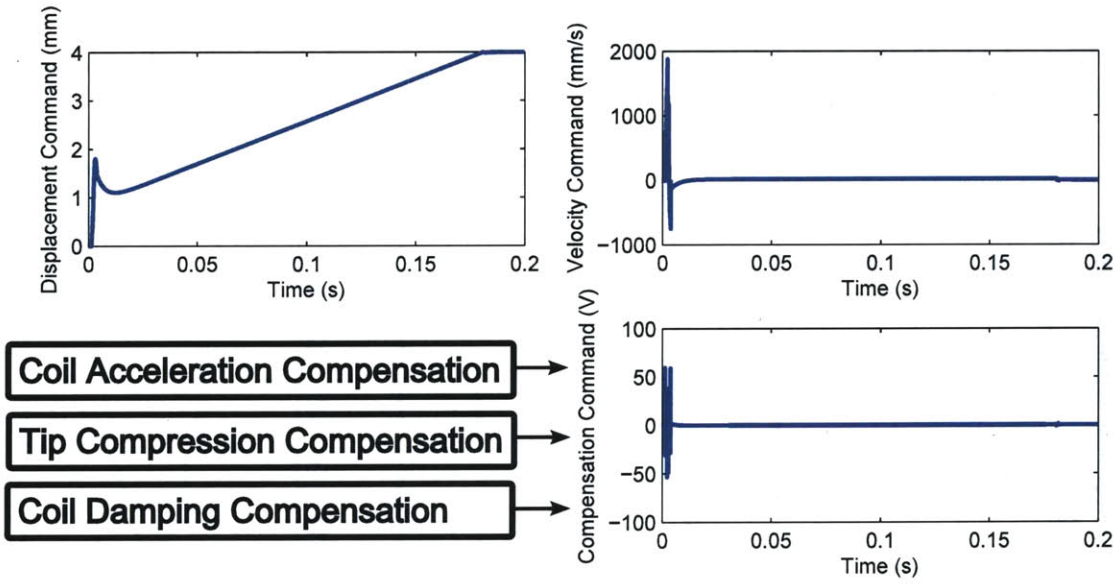

Figure 4-17: Graphs of three signals sent to FPGA for control, including the desired coil displacement, desired coil velocity, and a compensation command. The compensation command was the estimated input voltage required to follow the desired coil trajectory.

The FPGA was programmed to read the waveforms and output a voltage signal to the amplifier which is the sum of the displacement error multiplied by the P gain, the velocity error multiplied by the D gain, and a compensation command signal multiplied by compensation gain. These gains were manually tuned (starting from theoretically predicted values) to result in optimal waveform following. The calculation and output loop ran at 50 kHz, and the real-time velocity was predicted using a discrete derivative processed by a 2nd order 10 kHz Butterworth low-pass filter [46], resulting in a $\sqrt{1/2}$ attenuation of the real velocity at 10 kHz. Because our desired jet velocity time was 1 ms, we predicted minimal attenuation of error correction. The FPGA state-following algorithm is shown in Fig. 4-18. New Injex^{TM} ampoules were used for this section, with diameters averaging 193 µm.

4.3.2 Tip Estimation Controller Testing

The new controller successfully improved response of piston tip displacement using estimation techniques. As shown in Fig. 4-19, the desired path is followed by the coil but not by the piston. This is opposed to Fig. 4-20, where the estimated tip displacement is controlled, resulting in tip displacement waveform following.

The estimation controller exhibited a mean RMS error of 0.11 mm over 10 injections at v_{jet} 200 m/s; t_{jet} 1 ms; $v_{followthrough}$ 5 m/s; $V_{desired}$ 40 µL. If the desired displacement in the bang-PD controller is taken to be the desired tip displacement, the bang-PD controller exhibited RMS errors four times this amount. However, the controller still has room for improvement. The envelope plot shown in Fig. 4-21 shows the repeatability of the controller. As we zoom to the most dynamic section of the injection in Fig. 4-22, clear oscillations are seen about the set point.

4.3.3 Analysis Improvements

Several diagnostics are routinely run before and after needle eye injections, including IOP measurement, vision tests, and ophthalmoscope inspection. Additionally, before and after jet injection trials for other tissues types, samples are weighed to

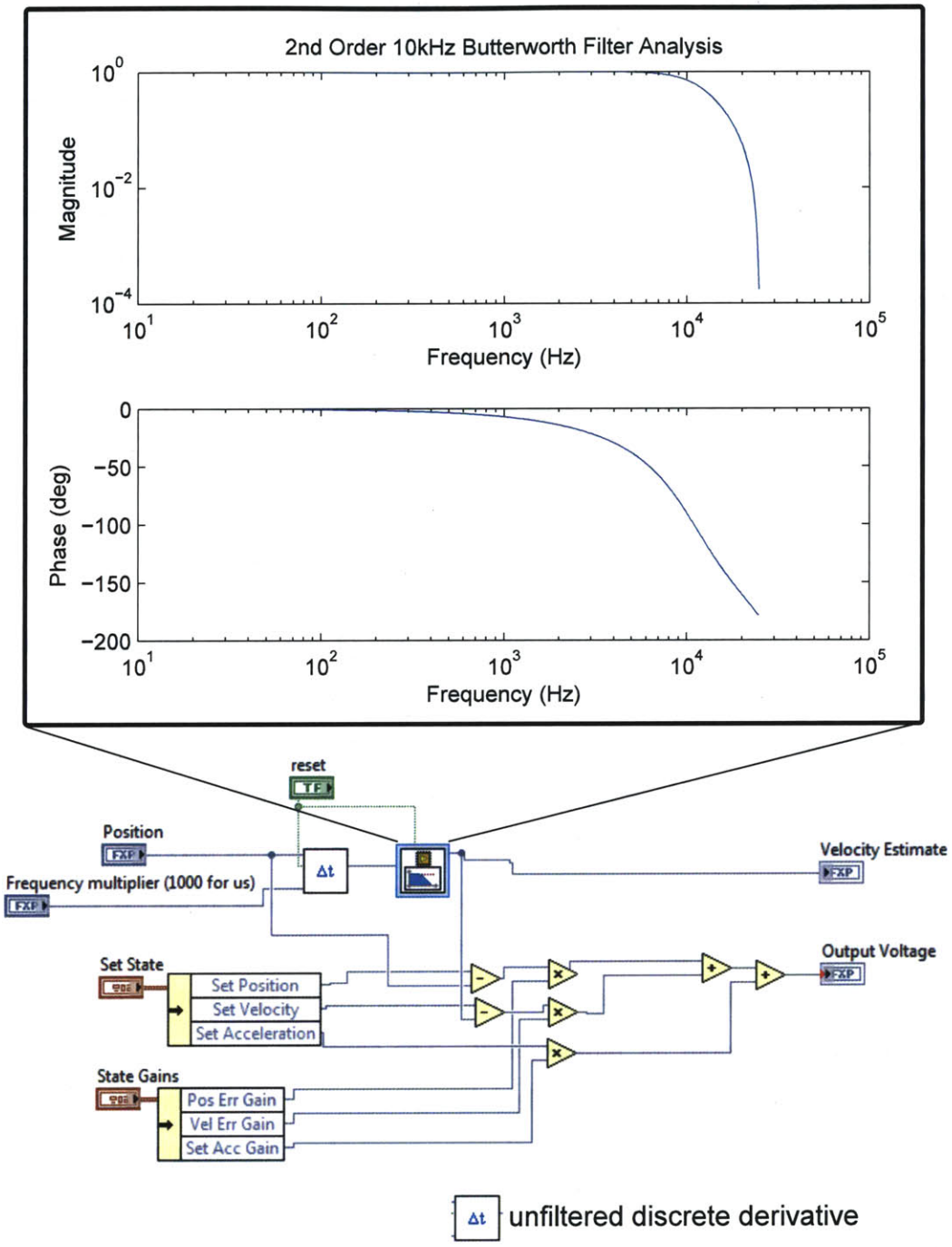

Figure 4-18: Diagram of full-state control algorithm, programmed in LabVIEW. The phase lag of the Butterworth filter was acceptable at the frequencies required for good trajectory following. (found to be $< 5\,\text{kHz}$).

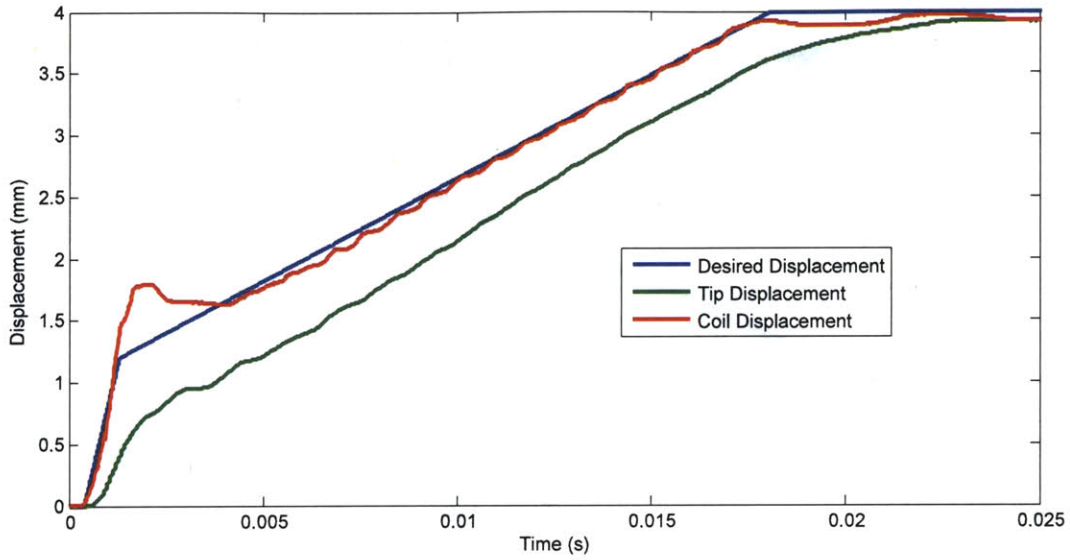

Figure 4-19: Comparison of desired, tip, and coil displacements for the bang-PD controller.

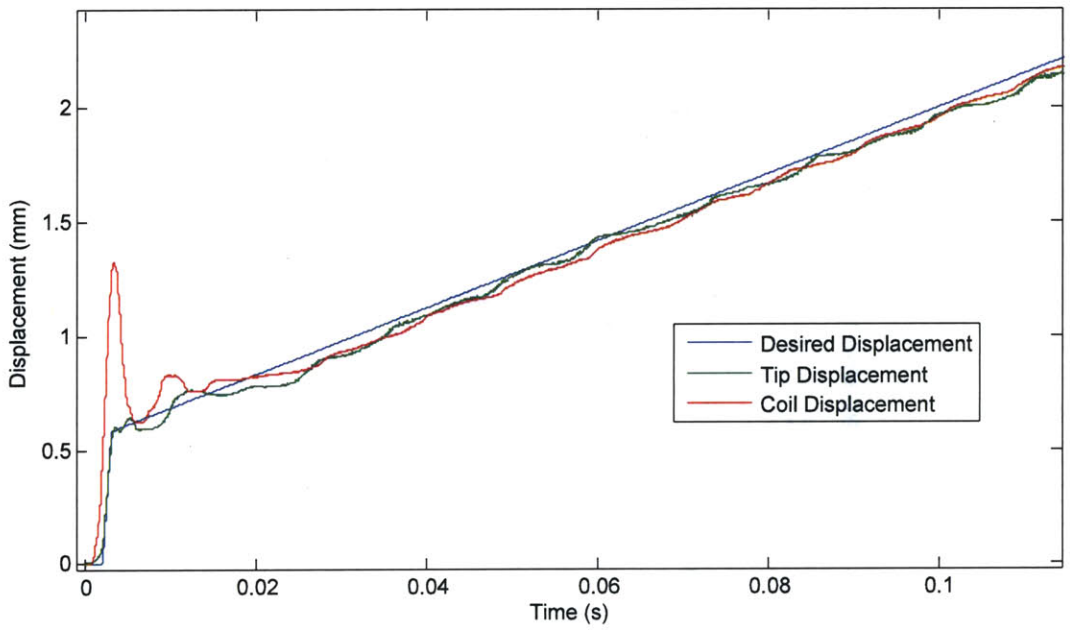

Figure 4-20: Comparison of desired, tip, and coil displacements for the tip estimation controller. v_{jet} 200 m/s; t_{jet} 1 ms; $v_{followthrough}$ 5 m/s; $V_{desired}$ 40 µL

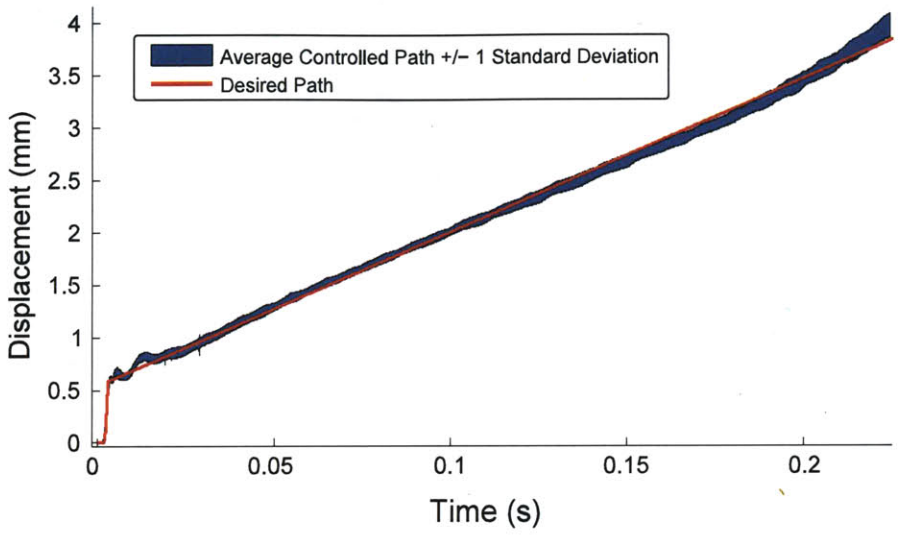

Figure 4-21: Tip estimation controller air injection trials. The video analysis software becomes less reliable towards the end of the injection stroke. v_{jet} 200 m/s; t_{jet} 1 ms; $v_{followthrough}$ 5 m/s; $V_{desired}$ 40 µL

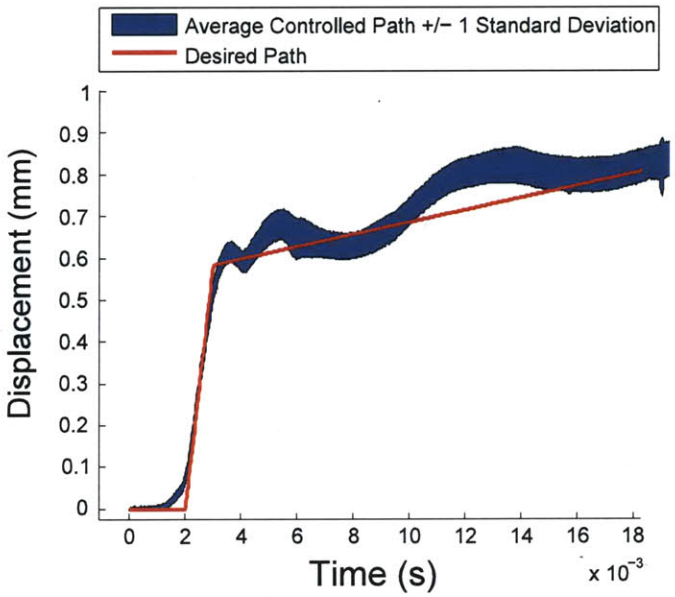

Figure 4-22: Zoomed section of dynamic region of Fig. 4-21.

estimate the total injection volume. Incorporating some of these techniques into IV JI experiments was one goal of this design iteration.

Before an IV JI trial, a sample was weighed and measured for IOP with a Shiotz tonometer (Riester 5112, Jungingen, Germany). Before weighing, the injection site of the eye was dried using a cotton wipe. After the injection, the injection site was again dried, the eye was weighed, measured for IOP, and inspected visually using a miniature ophthalmoscope (Riester 3012, Jungingen, Germany). Because we lacked a Schiotz tonometer calibration for rabbit eye IOP, all IOP measurements were relative. A 20 g mass was added to the Schiotz tonometer because the shape of the rabbit eye was not sufficiently deflected using the supplied masses for humans (up to 10 g).

4.3.4 Rabbit Eye Injection Testing

Eyes were injected in the same fashion as Section 4.2.3, except injection trials were performed within 1 hour of explanting using the new controller. The rabbits used in these studies had been given heparinized saline IV for several hours beforehand. Because the controller exhibited repeatable piston-tip following, controller parameters v_{jet}, t_{jet}, $v_{followthrough}$, and $V_{desired}$ were used for comparing eye injections. Several injections were non-penetrating, corresponding to v_{jet} settings less than or equal to 240 m/s and t_{jet} settings of 1 ms. It was found that a 240 m/s v_{jet} and 1.5 ms t_{jet} repeatedly penetrated eyes, and six injections were performed with varying $v_{followthrough}$ settings and 40 µL $V_{desired}$. These eyes were sectioned and measured for the metrics in Section 4.2.3. The results of these injections are plotted in Fig. 4-23.

Results suggested minimal influence of $v_{followthrough}$ at a v_{jet} of 240 m/s on both retinal tear diameter and entry hole diameter. As shown in Fig. 4-24, dye from one segment of the waveform reached the back of the eye, and dye from another segment remained in the entry area of the eye. One hypothesis was that the high-velocity stream reached and tore the retina, while the follow-through stream released medicine into the vitreous without penetrating to the back of the eye. This suggested that at lower v_{jet} and longer t_{jet}, such as 200 m/s for 1.5 ms, reliable non-damaging injection may occur. 3D injection reconstruction from eye sectioning, shown in Fig. 4-

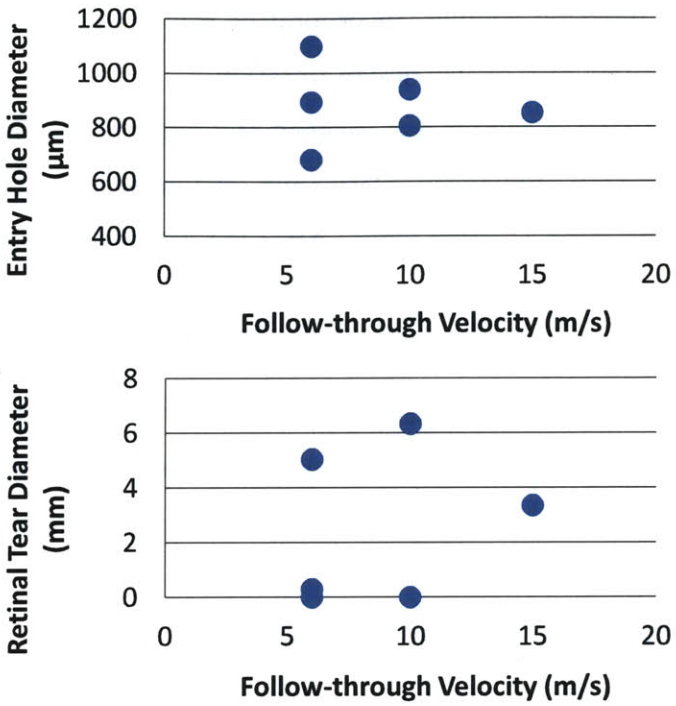

Figure 4-23: Retinal tear diameter and entry hole diameter as a function of $v_{followthrough}$. v_{jet} 240 m/s; t_{jet} 1.5 ms; $V_{desired}$ 40 µL.

25, illustrated that the bulk of dye delivered did not travel to the back of the eye, supporting the jet speed tearing hypothesis.

Energy put into the injection system was calculated by integrating the power at every time step of the injection. The power at each step was calculated by multiplying the amplifier voltage (V_{amp}) and current (I_{amp}). The energy used in same-parameter injection trials with torn and non-torn retinas differed by less than 5%, as shown in Fig. 4-26. This may indicate that varying biomechanical properties due to pre-injection treatment and handling (i.e. heparinization), not poor controller repeatability, were responsible for the distribution of retinal tearing among injections with the same parameters. This suggests that the injection parameters used lie in a region in which injections begin to cause damage.

Improvements in analysis were only used for the first six penetrated eyes, due to unrepeatable weighing with evaporation and steady IOP. By weighing several samples after sitting untouched for 5 minutes, minimum mass evaporated during a single protocol trial was estimated to be 19 mg with deviation on the same order as the

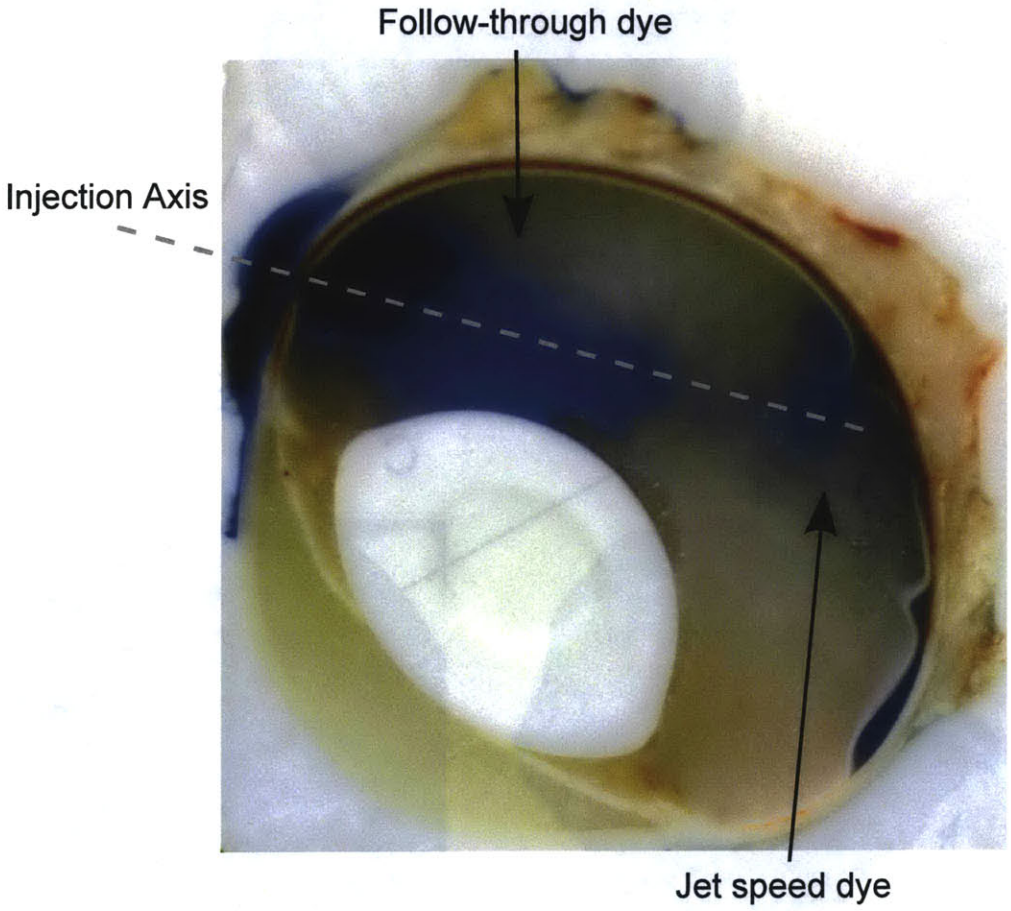

Figure 4-24: Hypothesized two-segment waveform effect on retinal tearing.

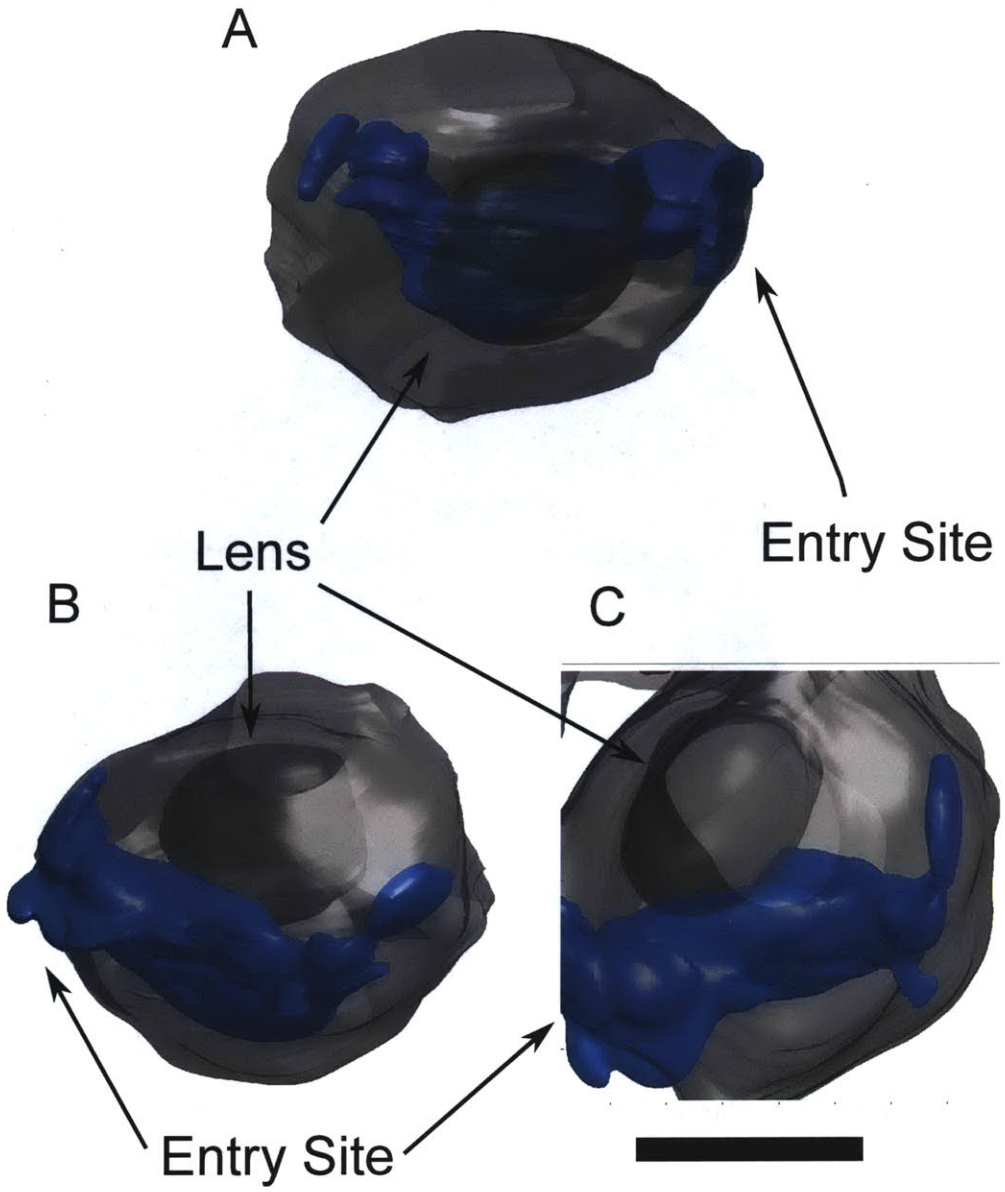

Figure 4-25: 3D reconstruction of eye structure and dye using 30 µm sections. The bulk of the injected dye did not reach the retinal tearing site. Scale bar is 10 mm. (A) Anterior medial view. (B) Posterior medial view. (C) Superior view.

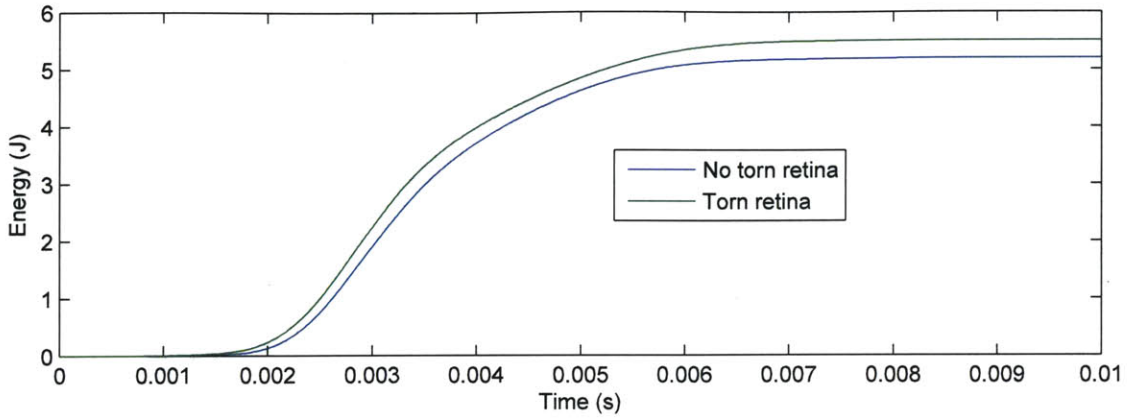

Figure 4-26: Energy comparison of two injections with the same parameters, one causing retinal damage, and the other leaving the retina intact.

mass of our injection volumes, rendering the metric unreliable for estimating mass injected. The first six penetrating injections had no effect on IOP at the resolution of the Schiotz tonometer, suggesting that differences in IOP are most accurately determined on live animals. The ophthalmoscope was subjectively useful, aiding in pre-sectioning injection examination. However, with our current level of experience using the miniature ophthalmoscope, we were unable to assess retinal damage before sectioning.

Chapter 5

Conclusions and Future Work

As of the last iteration of the IV JI, reliable needle free jet injection was not accomplished. However, several large strides were made in the direction of reliable injections. First, a controller was developed that allows the jet injector to more closely follow a jet velocity trajectory, especially for small volumes and high velocities. Second, staging and analysis tools developed in this thesis have provided insight into the modes of eye damage and the effects of altering various injection parameters. Finally, using this information, injection trials have steadily become more reliable and are expected to continue on this trend with future work. These injection trials have also highlighted several of the advantages of adapting jet injection technology to intravitreal injection stated in Section 4.1.

It is likely that reliable IV JI can be achieved using the hardware and software developed in this thesis, merely by making the parameter adjustments suggested in Section 4.3.4. If it is necessary to make further hardware or software changes, future work will focus on improving controller performance, injector mechanical design, and parameter selection. At the moment, the controller exclusively uses the coil position-piston tip transfer function for its feed-forward model. With high-speed fluid flow measuring techniques such as particle image or laser Doppler velocimetry, a model from coil position directly to jet velocity can be developed. Moreover, the addition of adaptive control will improve trajectory following from injection to injection. Mechanically, redesigning the ampoule nozzle geometry may decrease damage to the eye

by reducing the divergence and diameter of the exit stream. Finally, an optimized Lorentz-force actuator and a faster FPGA and real-time interface may improve control response and capabilities, increasing the options available for IV JI control.

Chapter 6

Bibliography

[1] Institut de la Vision, Paris, France. `www.institut-vision.org`.

[2] "Neurobiology 104 histology and cell biology - ora serrata histology." instructional material from Department of Neurobiology, School of Medicine, University of California, Los Angeles at `http://neuromedia.neurobio.ucla.edu/campbell/eyeandear/wp_images/175_ora_serrata.gif`.

[3] J. Park, P. M. Bungay, R. J. Lutz, J. J. Augsburger, R. W. Millard, A. S. Roy, and R. K. Banerjee, "Evaluation of coupled convective-diffusive transport of drugs administered by intravitreal injection and controlled release implant," *Journal of Controlled Release*, vol. 105, no. 3, pp. 279–295, 2005.

[4] J. C. Folk, "Eye intravitreal injection technique." instructional video at `http://www.medicalvideos.us/play.php?vid=1964`, Aug. 2010.

[5] A. Taberner, N. C. Hogan, and I. W. Hunter, "Needle-free jet injection using real-time controlled linear lorentz-force actuators," *Medical Engineering & Physics*, 2012, in press.

[6] A. J. Taberner, N. B. Ball, N. C. Hogan, and I. W. Hunter, "A portable needle-free jet injector based on a custom high power-density voice-coil actuator," in *Engineering in Medicine and Biology Society, 2006. EMBS '06. 28th Annual International Conference of the IEEE*, pp. 5001–5004, 2006.

[7] Y. Barak, M. D. Amiran, E. Fineberg, and Y. Lang, "Perforating eye injury caused by a dermojet syringe," *Archives of Dermatology*, vol. 145, no. 8, pp. 958–960, 2009.

[8] G. A. Peyman, K. Hosseini, and M. Cormier, "A minimally invasive jet injector for intravitreal and subconjunctival injection," *Ophthalmic Surgery, Lasers & Imaging*, vol. 43, no. 1, pp. 57–62, 2012.

[9] Futek, `www.futek.com`.

[10] P. V. Algvere, B. Sten, S. Seregard, and A. Kvanta, "A prospective study on intravitreal bevacizumab (avastin) for neovascular age-related macular degeneration of different durations," *Acta Ophthalmologica*, vol. 86, no. 5, pp. 482–489, 2008.

[11] J. O. Mason, P. A. Nixon, and M. F. White, "Intravitreal injection of bevacizumab (avastin) as adjunctive treatment of proliferative diabetic retinopathy," *Americal Journal of Ophthalmology*, vol. 142, no. 4, pp. 685–688, 2006.

[12] G. Sunaric-Mgevand and C. J. Pournaras, "Current approach to postoperative endophthalmitis.," *The British Journal of Ophthalmology*, vol. 81, no. 11, pp. 1006–1015, 1997.

[13] C. Shima, H. Sakaguchi, F. Gomi, M. Kamei, Y. Ikuno, Y. Oshima, M. Sawa, M. Tsujikawa, S. Kusaka, and Y. Tano, "Complications in patients after intravitreal injection of bevacizumab," *Acta Ophthalmologica*, vol. 86, no. 4, pp. 372–376, 2008.

[14] J. D. Bullock, R. E. Warwar, and W. R. Green, "Ocular explosion during cataract surgery: a clinical, histopathological, experimental, and biophysical study.," *Transactions of the American Ophthalmological Society*, vol. 96, pp. 243–281, 2008.

[15] P. Y. S. Chua, I. Mitrut, A.-M. Armbrecht, A. Vani, T. Aslam, and B. Dhillon, "Evaluating patient discomfort, anxiety, and fear before and after ranibizumab

intravitreous injection for wet age-related macular degeneration," *Archives of Ophthalmology*, vol. 127, no. 7, pp. 313–316, 2009.

[16] J. S. Pulido, M. E. Zobitz, and K.-N. An, "Scleral penetration force requirements for commonly used intravitreal needles," *Eye*, vol. 21, pp. 1210–1211, 2007.

[17] J. S. Pulido, C. M. Pulido, S. J. Bakri, C. A. McCannel, and J. D. Cameron, "The use of 31-gauge needles and syringes for intraocular injections," *Eye*, vol. 21, pp. 829–830, 2007.

[18] T. W. Olsen, S. Y. Aaberg, D. H. Geroski, and H. F. Edelhauser, "Human sclera: Thickness and surface area," *American Journal of Ophthalmology*, vol. 125, no. 2, pp. 237–241, 1998.

[19] T. R. Friberg and J. W. Lace, "A comparison of the elastic properties of human choroid and sclera," *Experimental Eye Research*, vol. 47, no. 3, pp. 429–436, 1988.

[20] R. E. Norman, J. G. Flanagan, S. M. Rausch, I. A. Sigal, I. Tertinegg, A. Eilaghi, S. Portnoy, J. G. Sled, and C. R. Ethier, "Dimensions of the human sclera: Thickness measurement and regional changes with axial length," *Experimental Eye Research*, vol. 90, no. 2, pp. 277–284, 2010.

[21] J. Black, *Handbook of Biomaterial Properties.* Thomson Science, 2–6 Boundary Row, London SE1 8HN, UK: Chapman & Hall, 1 ed., 1998.

[22] J. Xu, J. J. Heys, V. H. Barocas, and T. W. Randolph, "Permeability and diffusion in vitreous humor: Implications for drug delivery," *Pharmaceutical Research*, vol. 17, 2000.

[23] C. G. Wilson, L. E. Tan, and J. Mains, "Principles of retinal drug delivery from within the vitreous," in *Drug Product Development for the Back of the Eye* (U. B. Kompella, H. F. Edelhauser, and D. J. A. Crommelin, eds.), vol. 2 of *AAPS Advances in the Pharmaceutical Sciences Series*, pp. 125–158, Springer US, 2011.

[24] D. R. Anijeet, R. J. Hanson, J. Bhagey, and R. A. Bates, "National survey of the technique of intravitreal triamcinolone injection in the united kingdom," *Eye*, vol. 21, pp. 480–486, 2006.

[25] J. F. Korobelnik, M. Weber, S. Y. Cohen, and E. Panel, "Guidelines for intravitreal injections," *Journal Franais DOphtalmologie*, vol. 32, pp. e1–e2, 2009.

[26] B. Hemond, "A lorentz-force actuated controllable needle-free drug delivery system," Master's thesis, Massachusetts Institute of Technology, Cambridge, Massachusetts, Feb. 2006.

[27] National Instruments LabVIEW, `www.ni.com/labview/`.

[28] D. Wendell, B. Hemond, N. Hogan, A. Taberner, and I. Hunter, "The effect of jet parameters on jet injection," in *Engineering in Medicine and Biology Society, 2006. EMBS '06. 28th Annual International Conference of the IEEE*, pp. 5005–5008, 2006.

[29] H. T. Perry, B. T. Cohn, and J. S. Nauheim, "Accidental intraocular injection with dermojet syringe," *Archives of Dermatology*, vol. 113, no. 8, p. 1131, 1977.

[30] P. A. Tsonis, ed., *Animal models in eye research.* Academic Press, 2008.

[31] N. Lassota, J. U. Prause, E. Scherfig, J. F. Kiilgaard, and M. La Cour, "Clinical and histological findings after intravitreal injection of bevacizumab (avastin) in a porcine model of choroidal neovascularization," *Acta Ophthalmologica*, vol. 88, no. 3, pp. 300–308, 2010.

[32] S. J. Bakri, J. D. Cameron, C. A. McCannel, J. S. Pulido, and R. J. Marler, "Absence of histologic retinal toxicity of intravitreal bevacizumab in a rabbit model," *American Journal of Ophthalmology*, vol. 142, no. 1, pp. 162–164, 2006.

[33] P. Heiduschka, H. Fietz, S. Hofmeister, S. Schultheiss, A. F. Mack, S. Peters, F. Ziemssen, B. Niggemann, S. Julien, K. U. Bartz-Schmidt, and U. Schraermeyer, "Penetration of bevacizumab through the retina after intravitreal in-

jection in the monkey," *Investigative Ophthalmology & Visual Science*, vol. 48, pp. 2814–2823, 2007.

[34] F. Lu and R. Adelman, "Are intravitreal bevacizumab and ranibizumab effective in a rat model of choroidal neovascularization?," *Graefe's Archive for Clinical and Experimental Ophthalmology*, vol. 247, pp. 171–177, 2009.

[35] J. C. Downs, J. K. Suh, K. A. Thomas, A. J. Bellezza, C. F. Burgoyne, and R. T. Hart, "Viscoelastic characterization of peripapillary sclera: material properties by quadrant in rabbit and monkey eyes," *Journal of Biomechanical Engineering*, vol. 125, pp. 124–131, 2003.

[36] R. Beuerman, A. Barathi, S. Weon, and D. Tan, "Two models of experimental myopia in the mouse," *Investigative Ophthalmology & Visual Science*, vol. 44, p. 4338, 2003.

[37] *Encyclopdia Britannica. Encyclopdia Britannica Online.*, ch. fluid mechanics. Encyclopdia Britannica Inc., 2012.

[38] Vision Research, Wayne, New Jersey. `www.visionresearch.com`.

[39] Injex Pharma Ltd., Miama, FL. `www.injex.com`.

[40] AE Techron, Elkhart, IN. `www.aetechron.com`.

[41] National Instruments, Austin, TX. `www.ni.com`.

[42] Texas Instruments, Dallas, TX. `www.ti.com`.

[43] Dolan-Jenner, Lawrence, MA. `www.dolan-jenner.com`.

[44] MathWorks MATLAB, `www.mathworks.com/products/matlab/`.

[45] S. Ding, "Recent developments in ophthalmic drug delivery," *Pharmaceutical Science & Technology Today*, vol. 1, no. 8, pp. 328 – 335, 1998.

[46] S. Butterworth, "On the theory of filter amplifiers," *Experimental Wireless & the Wireless Engineer*, vol. 7, pp. 536–541, 1930.